Review Article

Calibration and Validation of Confocal Spectral Imaging Systems

Jeremy M. Lerner[1]* and Robert M. Zucker[2]

[1]LightForm, Inc., Hillsborough, New Jersey

[2]U.S. Environmental Protection Agency, Reproductive Toxicology Division, National Health and Environmental Effects Research Laboratory, Research Triangle Park, North Carolina

Received 13 April 2004; Revision Received 26 July 2004; Accepted 26 July 2004

Background: Confocal spectral imaging (CSI) microscopic systems currently on the market delineate multiple fluorescent proteins, labels, or dyes within biological specimens by performing spectral characterizations. However, some CSI systems have been found to present inconsistent spectral profiles of reference spectra within a particular system and between related and unrelated instruments. This variability confirms that there is a need for a standardized, objective calibration and validation protocol.

Methods: Our protocol uses an inexpensive multi-ion discharge lamp (MIDL) that contains Hg^+, Ar^+, and inorganic fluorophores that emit distinct, stable, spectral features in place of a sample. We derived reference spectra from the MIDL data to accurately predict the spectral resolution, ratio of wavelength to wavelength, contrast, and aliasing parameters of any CSI system. We were also able to predict and confirm the influence of pinhole diameter on spectral profiles.

Results: Using this simulation, we determined that there was good agreement between observed and theoretical expectations, thus enabling us to identify malfunctioning subsystems. We examined eight CSI systems and one non-confocal spectral system, all of which displayed spectral inconsistencies. No instrument met its optimal performance expectations. In two systems, we established the need for factory realignment that had not been otherwise recognized.

Conclusions: We found that using a primary light source that emits an absolute standard "reference spectrum" enabled us to diagnose instrumental errors and measure accuracy and reproducibility under normalized conditions. With this information, a CSI operator can determine whether a CSI system is working optimally and make objective comparisons with the performance of other CSI systems. We determined that, if CSI systems were standardized to produce the same spectral profile of a MIDL lamp, researchers could be confident that the same experimental findings would be obtained on any CSI system.

Key terms: confocal microscope; wavelength calibration; spectral calibration; spectral imaging; Zeiss; Leica; SKY; PARISS; quality assurance; validation; photomultiplier tube

Abbreviations: AOBS: Acousto optic beam splitter; AOTF: Acousto optic tunable filter; BP: Bandpass; BPF: Bandpass filter; BFP, Blue fluorescent plastic; CCD, Charge coupled device; CSI, Confocal spectral imaging; CV, Coefficient of variation; DRS, Derived reference spectrum; FWHM, Full width at half maximum; FOV, Field of view; GSU, Gray scale unit; IPMT, Imaging photo-multiplier tube; LCSI, Leica confocal spectral imaging; LCTF, Liquid crystal tunable filter; MIDL, Multi ion discharge lamp; OCSI, Olympus confocal spectral imaging; PFOV, Point in the field of view; PMT, Photo multiplier tube; PVR, Peak to valley ratio; QE, Quantum efficiency; RBF, Red bandpass filter; RLD, Relative linear dispersion; SCF, Spectral characterization functions; SDP, Spectral dispersion plane; S/N, Signal to noise ratio; WDE, Wavelength dispersive element; WSI, Wavelength sampling increment; WDP, Wavelength data point; WTWR, Wavelength to wavelength ratio; ZCSI, Zeiss confocal spectral imaging.

The research described in this article has been reviewed and approved for publication as an EPA document. Approval does not necessarily signify that the contents reflect the views and policies of the Agency, nor does mention of trade names or commercial products constitute endorsement or recommendation for use.

*Correspondence to: Jeremy M. Lerner, LightForm, Inc., 601 Route 206, Suite 26-479, Hillsborough, NJ 08844.

E-mail: jlerner@lightforminc.com

Published online 5 October 2004 in Wiley InterScience (www.interscience.wiley.com).

DOI: 10.1002/cyto.a.20087

Traditional confocal microscopy systems are designed to detect the location and intensity of various fluorophores that may be present within a sample by taking intensity measurements through a dielectric bandpass filter (BPF; also referred to as a barrier filter). This BPF allows a relatively large spectral segment (typically >40 nm) to pass to a photomultiplier tube (PMT) that measures the intensity of the emission. Simplistically, to characterize multiple fluorophores, various BPFs can be exchanged sequentially or a number of PMT assemblies can operate simultaneously, each with its own unique BPF. Filter techniques work well when the spectral emission characteristics of targeted fluorophores do not overlap with the emission profiles of other fluorophores.

In real life, autofluorescence, natural fluorophores, and an increasing need to work with multiple human-made fluorophores, many with overlapping spectral profiles, have led to the development of a new family of instruments that acquire an extended wavelength range. In this report, we use as examples three laser-based confocal spectral imaging (CSI) systems produced by Leica (LCSI), Zeiss (ZCSI), and Olympus (OCSI). Whereas classic confocal systems acquire a single wavelength data point (WDP), determined by the characteristics of a BPF, these systems use a wavelength dispersive spectrometer to acquire a series of WDP to cover the entire spectral range.

Natural spectra are analog and change continuously with wavelength as a function of intensity. For a digital spectrum to be equivalent to an analog spectrum, it requires an infinitely large number of WDPs, each with an infinitely narrow spectral width. CSI systems are digital, so they acquire a finite number of WDPs, each with a finite spectral width. As a consequence, CSI systems only "sample" the spectral range. In an otherwise perfect system, the accuracy and specificity of the resulting spectral reconstruction is a function of the number of WDPs and their wavelength sampling increment (WSI; or spectral width). Depending on the make and model, the WSI of a CSI system is roughly equivalent to the "bandpass" of a BPF and can vary between 2 and 11 nm.

It should be evident that the integrity of a spectral image depends on the integrity of a spectral reconstruction; as a consequence, we were troubled that that many of the CSI systems we tested (individual systems and not particular CSI manufacturers or models) presented unexpected spectral distortions and inaccuracy. CSI systems present the opportunity to help researchers gain insight into complex cellular systems; however, unless good accuracy and precision can be assured, pathways that may be suggested by shifts or changes in spectral characteristics may become difficult, if not impossible, to determine. Regrettably, pictures can be passed as "insight" (1), effectively bypassing objectivity in favor of subjectivity.

With these issues in mind, this study was initiated when we observed inconsistent spectral profiles from the same emission source within a Leica TCS-SP1 at the U.S. Environmental Protection Agency (USEPA). The manufacturer did not provide a meaningful benchmark that could be used to validate the integrity of a spectral acquisition from the system. As a result, it became increasingly difficult to determine whether we were observing changes in our specimens or the instrument hardware. We knew from previous experience that flow cytometers and traditional confocal laser scanning microscopic systems present variables that can be characterized with standard samples, such as fluorescent beads of different types and sizes, to determine the coefficient of variation, spectral registration, field illumination, laser stability and power, and axial registration (2–6). The tests that follow help complete the set of diagnostic tools needed to perform a full characterization of any confocal system that incorporates spectral mapping functions. The tests that are described in this report require that the CSI system being characterized be operating optimally in conventional confocal imaging mode (nonspectral).

A major emphasis of this report is the prediction of the theoretical spectral profile of a standard wavelength calibration light source for each instrument and the comparison of its predicted spectral profile with that observed experimentally. We include a tutorial Appendix that describes the practical considerations of the optics of spectroscopy and the effects of certain hardware functions on the performance expectations of a CSI system.

The Appendix covers the spectroscopic definitions and how to calculate "resolution" and "bandpass," which may be different from those used by some researchers in the imaging community. We describe how bandpass changes with the numerical aperture (NA) and magnification of the microscope objective, and how the WSI limits, but does not determine, bandpass. We also include a section on light "throughput" from a geometric optics standpoint that shows how fluorescent intensity depends more on the area of the pinhole than on the size of the Airy disk.

This report is written from a spectroscopic point of view; as a consequence, we are interested in being able to measure not only the full width at half maximum (FWHM) of an emission but also the shape of the spectral profile. In reality, few, if any, organic fluorophores emit a single symmetric gaussian or lorentzian profile. When multiple fluorophores overlap, we often observe a complex emission spectral profile with a single maximum and shoulders due to multiple spectral components that make up the composite emission. As a consequence, a goal of a spectral characterization must be to generate enough detail to be able to accurately identify these often subtle features. Because a CSI system converts spectroscopic information into an image, the value of the image depends on the accuracy of a spectral reconstruction. This report will help a CSI operator to understand and determine how CSI hardware contributes to the spectral profile of a fluorophore and the consequences of certain user decisions concerning the system setup. We hope to enable a researcher to assess the integrity of spectroscopic data acquired on a CSI system and to diagnose which problems are resolvable and which are not. To do this, we provide a protocol that enables the user to determine whether a CSI system is in good optomechanical alignment and whether its spectral resolution meets objective expecta-

tions when tested against an absolute calibration standard. We consider that a CSI system is performing well when it produces an appropriate spectral characterization of a true reference spectrum.

Just as an image produced by a digital camera incorporates inherent contributions from read noise, shot noise, and dark noise (all factors that most researchers recognize), a spectrometer contributes inherent properties that deform acquired spectra but are typically unrecognized. To determine the spectral accuracy of a CSI system, it is necessary to accommodate the natural profile of the spectral emission, contributions from instrumental factors that include limitations on its ability to measure bandpass and resolution, "instrumental artifacts" due to inherent wavelength sampling errors (aliasing), and errors due to misalignment or defocusing.

Aliasing can affect the ability to "unmix" commingled spectra, as opposed to spatially separated fluorophores that present overlapping spectra. Changes in the shape of a spectrum can compromise chemometric unmixing algorithms and limit their ability to accurately assess the spectral components of the mixture (7).

By using a multi-ion discharge lamp (MIDL) as a primary absolute standard to replace the sample on a microscope stage, we were able to devise a series of tests to accurately quantify instrumental functions to determine acceptable performance and point to evidence of system malfunction. An acquired calibration spectrum can then be evaluated in the following terms.

- Spectral resolution or bandpass to determine the contribution of an instrument to an acquired spectral profile. Whenever the term "bandpass" is used in this report, it refers to the determination of the FWHM of a spectral emission from the field of view (FOV).
- Peak-to-valley ratios (PVR) to objectively test contrast.
- Wavelength-to-wavelength ratios (WTWR) to provide a means of confirming that an instrument is capable of making accurate wavelength ratio measurements.
- Aliasing (due to undersampling the emitted spectrum) that may be responsible for nonlinear and significant errors in an observed spectral profile.
- The contribution of pinhole diameter to a spectral profile.

Consultation with other CSI owners has confirmed that few, if any, manufacturers of CSI instruments provide verifiable performance specifications that define the ability of the instrument to reconstruct a spectrum emitted by a wavelength calibration standard. Fortunately, the research analytical spectroscopy community developed such tools more than 60 years ago with primary multi-ion emission wavelength calibration lamps that were readily available and inexpensive, such as the MIDL. The spectral characteristics of their emission profiles, including their natural line widths, are known to many decimal places. By using the MIDL light source, we can mathematically model the theoretical ability of any CSI system (or any spectrometer) to reconstruct the MIDL spectral profile. With this model, we were able to compare observed with theoretical spectral profiles for almost any WSI a CSI system may offer. The narrow emission line width of the spectral features of the MIDL makes it well suited for all research-quality instruments with a WSI from 1 to 12 nm. This includes all LCSI, ZCSI, and OCSI systems and most, if not all, interferometer and high-end liquid crystal tunable filter and acousto-optic tunable filter systems. The spectral line widths of the MIDL lamp are too narrow to be effective with low-resolution spectral systems with a WSI larger than 12 nm due to the inherent inaccuracy of a fit. We tested our calibration and validation protocol on seven CSI instruments and one nonconfocal system. The goals of this report are to (a) encourage manufacturers and instrument operators to adopt standardized spectral evaluation tests that will enhance the level of communication between colleagues and manufacturers, (b) provide an accurate and rapid test that determines whether a CSI system is operating correctly, and (c) provide standards that can be used by the confocal community to ensure the accuracy of their research findings and thus validate their acceptability and credibility.

In this report, all spectra are shown background subtracted and normalized to unity unless otherwise indicated.

MATERIALS

Certified Spectral MIDLs

There are several readily available calibration sources, the most common of which is a low-pressure Hg^+/Ar^+ discharge lamp that covers the wavelength range of 400 to 840 nm. The emission spectrum of this lamp is shown in Figure 1a (Spectroline, Spectronics Corp., Westbury NY, and Oriel Corp., Stratford CT supply a wide variety of wavelength calibration lamps). The main drawback of pure Hg^+/Ar^+ lamps is that they emit deep ultraviolet light that is dangerous to exposed skin and can cause blindness to unprotected eyes. Hence, we use an eye-safe, MIDL distributed by LightForm, Inc. (Hillsborough, NJ). The MIDL presents monochromatic emission features emitted by Hg^+, Ar^+, and narrow, but not monochromatic, inorganic fluorophores to cover the spectrum from 400 to 840 nm (Fig. 1b). The lamp emits down to 365 nm, but the intensity is weak, and it is not discussed further.

The MIDL (and Hg lamps in general) use Ar as a catalyst to initiate the Hg spectrum. As the lamp warms up, the Ar features that appear at greater than 650 nm typically disappear within 20 s of initiation of the Hg^+ emission. If the CSI system is capable of taking an entire spectrum in a single shot, this is not a problem; however, CSI systems that take wavelength data sequentially take such a long time to acquire the spectral data that the Ar^+ features disappear before a full spectrum can be acquired (this has the same net effect as photobleaching).

The MIDL is battery operated and emits light from a 6-mm-diameter "pencil" tube that replaces the sample on the microscope stage. Table 1 lists selected Hg^+, Ar^+, and

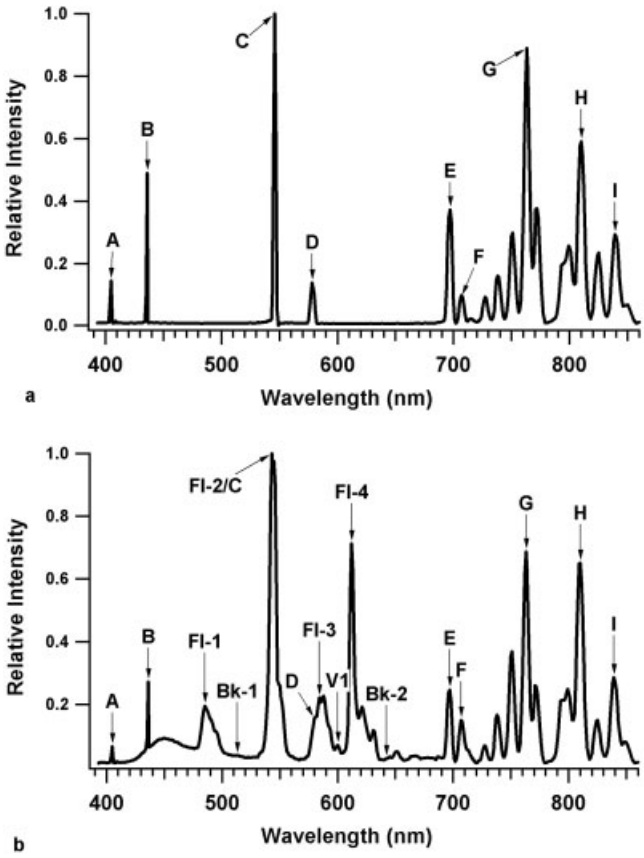

FIG. 1. Spectra of two calibration light sources: (**a**) pure Hg/Ar low-pressure discharge lamp and (**b**) LightForm MIDL. Both spectra are as presented and digitized by the PARISS spectrometer.

fluorophore emission features that correspond to the letters in Figures 1a and 1b.

The benefit of a MIDL spectrum is that it emits a spectral fingerprint that can be used to calibrate the performance of any spectroscopic system. A full listing of wavelength emission features can be obtained from the National Institute of Standards and Technology (8).

Calibration Lamp Certification

Calibration certificates showing the spectral profiles of these lamps were acquired with the PARISS spectral imaging system (LightForm, Inc.). PARISS is a prism-based, analytical wavelength dispersive system that acquires each spectrum with 640 WDPs. The spectral data are linearized with wavelength and corrected for a WSI of 1 nm. The data are stored in ASCII format in an Excel file (Microsoft, Redmond, WA). The raw data were acquired with an average WSI of 0.6 nm over 400 to 800 nm. Because most CSI systems acquire spectral data with considerably larger WSIs (5 to 20 times greater), a WSI of 1 nm is appropriate. ASCII files of MIDL data are provided with the lamp in pure form (nonlinearized, pixel vs. intensity) and after conversion to wavelength versus intensity (9).

766.5-nm Red Bandpass Filter (RBF)

Because the Ar^+ features at greater than 650 nm disappear rapidly, CSI systems such as the LCSI and OCSI take too long to acquire a full spectrum that includes the red region of the spectrum. For that reason, we use a 25-mm-diameter, 10-nm BPF with a center wavelength at 766.5 nm (part no. 079-1670, OptoSigma, Santa Ana, CA). (Dielectric BPFs can be used for making quick relative tests, but they should not be used for resolution tests or for the determination of wavelength accuracy. These devices are strictly secondary standards designed for use in collimated light).

Blue Fluorescent Plastic (BFP) Slides

A BFP (Applied Precision Inc., Issaquah, WA) was selected from a set of fluorescent plastic slides of various excitation and emission characteristics. The BFP was excited at 408 nm, and an emission spectrum with a maximum at 440 nm was used to characterize emission spectra in the blue region of the spectrum. Chroma Corporation (Brattleborough, VT) also makes acceptable fluorescent plastic slide sets.

Sperm

Hamster sperm was acquired from the epididymis and then suspended in 0.1% non-ionic detergent buffer (NP40) in a phosphate buffered saline buffer that contained 1 to 10 μg/ml of 4′,6-diamidino-2-phenylindole dihydrochloride (DAPI; NPE, Miami, FL).

The samples were placed on a slide covered with no. 1.5 coverglass, sealed, and analyzed with a water immersion lens (63×, NA 1.2).

PMT-LCSI

The sensitivity of a PMT changes as a function of its quantum efficiency (QE) at each wavelength. The LCSI system uses a Hamamatsu (Tokyo, Japan) R6358 PMT for PMT 1, rated for use from 185 to 800 nm, with a peak QE

Table 1
Peak Maxima for Principal Spectral Features in the Calibration Light Source

	Wavelength (nm)	Emission
A	404.7	Hg
B	435.8	Hg
C	546.0	Hg
D	577/579	Hg
E	696.5	Ar
F	706.7	Ar
G	763.5	Ar
H	811.5	Ar
I	840.8	Fluorophore
F1-1	485.0	Fluorophore
F1-2	544.0	Fluorophore
F1-3	586.0	Fluorophore
F1-4	611.5	Fluorophore
V1	605.0	Valley
Bk1	525	Background
Bk2	642	Background

at 530 nm and very low noise. PMTs 2 and 3 use Hamamatsu R6357 meshless PMTs (better for small illumination spot sizes), rated from 185 to 900 nm, with a peak QE at 450 nm. The photocathodes of PMTs 1 and 2 are nominally 13 × 4 mm (10).

PMT-ZCSI

The ZCSI uses a multi-anode 32-channel linear array H7260 imaging PMT (IPMT) as the wavelength detector (10). The IPMT is rated for use from 185 to 650 nm, with a peak QE at 420 nm. There are 32 channels, each 0.8 × 7 mm on 1-mm centers. In addition, there are two R6358 PMTs that are used for classic nonspectral confocal imaging.

Spectral Imaging Systems Tested

The validation and calibration protocol was developed for any spectral imaging system, whether or not it is confocal.

Confocal systems. We fully tested two Leica TCS-SP1 systems and one Leica TCS-SP2 system (Leica, Heidelberg, Germany) and four Zeiss LSM-510 Meta systems (Zeiss, Thornwood, NY). An Olympus FV1000 (Olympus, Melville, NY) was partly characterized.

Nonconfocal systems. The interferometer-based spectral imager (Applied Spectral Imaging [ASI], Carlsbad, CA) nonconfocal spectral imaging system, called the SKY spectral imager, covered the emission wavelength range from 400 to 900 nm. The SKY system is based on an ASI SD-300 Sagnac interferometer and a VDS-1300, 12-bit digital charge couple device (CCD) camera (1,280 × 1,024 pixels, usually operated in 2 × 2 binning mode) that covers the wavelength range from 400 to 900 nm and was mounted on a Leica (Wetzlar, Germany) DMRXA/RF-8 upright fluorescence automated microscope. Spectral images were acquired with S.I. 2.5 spectral imaging software (ASI) and analyzed in SpectraView 1.0 SKY system (ASI). Lenses included HC Plan 10×/0.40 PH1 A and HC Plan 20×/0.70 PH2C.

EXPERIMENTAL METHODS

Data Acquisition

The CSI system was first confirmed to be operating optimally in standard confocal mode. The field illumination of the lamp was adjusted so that there was approximately equal intensity throughout the image. All spectral acquisitions were optimized for signal-to-noise (S/N) level by adjusting the voltage to the PMTs to ensure a compromise signal level of ~100 gray-scale units (GSU; of a maximum of 256 GSU) and a positive background of ~5 GSU on the entire image to ensure that no weak signal would be truncated. The background was subtracted during data analysis.

Scans of wavelength versus intensity were acquired on LCSI systems ("lambda scans") with 50 sequential WDP acquisitions, each with a stated WSI of 5 nm from 400 to 650 nm. The lasers were turned off and the dichroic mirror was replaced with a 30/70 reflector. The MIDL was used to characterize system performance in the blue and visible regions. A 10-nm RBF BPF with a center wavelength at 766.5 nm, illuminated in brightfield with a halogen lamp, was used to characterize the region between 680 and 780 nm with 20 WDP.

ZCSI systems acquired spectra of the MIDL calibration source in 88-nm segments whereas each segment is a "bin" of 10.7 nm. The wavelength range from 462 to 665 nm took 20 WDPs and that from 462 to 794 nm took 32 WDPs. Voltage to the PMT was optimized to provide an optimum S/N ratio centered at 545 nm. The background offset was subtracted during data analysis.

Table 2
PARISS Spectral Characterization Functions

	WSI	WTWR	PVR	FWHM (F1-2)	FWHM (F1-4)
PARISS (400–800 nm)	1	0.7	35	6	4

Wavelength and Spectral Characterization Using a Calibration Lamp

The calibrated MIDL can be used for upright and inverted microscopes by placing the lamp under or over the objectives positioned to produce a uniformly illuminated FOV. The microscope objective can then be focused to yield maximum intensity. We used 10× and 20× objectives for the tests that follow. A scan of wavelength versus intensity is acquired by using the lamp as the sample. The lamp provides a very stable spectral output of 400 to 650 nm. The data from all spectral acquisitions were digitized, saved in ASCII format, and exported to Excel.

SPECTRAL CHARACTERIZATION FUNCTIONS

There are three basic spectral characterization functions (SCFs): FWHM, PVR, and WTWR. To determine these parameters for a given CSI system, the spectrum of the MIDL is acquired and analyzed. The spectra obtained will be a degraded variant of that shown in Figure 1b, if the WSI of the instrument is larger than 1 nm. The MIDL emission, as characterized by the PARISS spectral imaging system, provides the original reference spectrum with the SCFs listed in Table 2.

Spectral FWHM

Spectral FWHM was calculated by using the method described and defined as a function of bandpass in the Appendix (Spectrometer Operating Characteristics). Higher resolution and greater contrast require the narrowest possible FWHM.

Peak-to-Valley Ratio

PVR determines "contrast" and the ability of a system to differentiate between two close emission features that are significantly different in intensity or that overlap. Spectral resolution and background scatter contribute to the PVR value.

PVR measurements using the MIDL are taken in the valley at V1 between Fl-3 and Fl-4. The peak intensity is measured at Fl-4 (Fig. 1b). The actual PVR is then calculated by the ratio (Fl-4 − Bk2)/(V1 − Bk2), where Bk2 is the background measured at 660 nm (where there are no line emissions from the lamp). This test does not measure S/N ratio. The goal is to obtain the highest possible PVR value.

Wavelength-to-Wavelength Ratio

The WTWR is calculated as (Fl-4 − Bk2)/(Fl-2 − Bk1). The WTWR is determined by dividing the background-subtracted values of the peak intensity at Fl-4 by the background subtracted peak intensity at Fl-2. Because researchers frequently compare the peak intensity of one wavelength with another, this is an important test (11,12).

ALIASING

All naturally occurring spectra are analog waveforms. Therefore, if a fluorophore emits light over a given spectral range, it is continuous in wavelength and intensity. The goal of a spectral acquisition is to capture and reconstruct this waveform (or spectral profile) as accurately as possible. However, because we use a computer for data analysis, the analog waveform with an infinite number of WDPs, each with an infinitely fine WSI, must be converted into a digital format with a limited number of discrete data points and finite WSIs by wavelength "sampling." Aliasing occurs when the number of acquired WDPs is insufficient to accurately reconstruct an analog spectrum (13). Therefore, the largest number of WDPs with the smallest WSIs will result in the most accurate spectral reconstruction. In a CSI system, the number of WDPs may be limited by the WSI options available to the user; therefore, some aliasing is inevitable and is then a systematic error.

In classic imaging, if the image of a curved edge acquired by a digital camera is represented by "jagged" edges (artifacts), then the curve was undersampled. This is an example of aliasing. There are antialiasing imaging tools that attempt to fill in the "gaps" to "smooth" the edges to make a more *subjectively* pleasing appearance (14). However, antialiasing techniques do not correct underlying errors because they almost always add data that corrupt the raw original dataset. An XY scatter graph that connects data points with a smoothed line is a form of antialiasing. This presentation creates an appearance that is subjectively more attractive, but the resulting curve can be misleading; therefore, all spectra shown in this reported were drawn point to point without interpolation or smoothing.

According to the Nyquist theorem, if naturally occurring spectra are periodic, the original analog signal (a spectrum in this case) should be "sampled" with at least twice the frequency of the original. Unfortunately, natural spectra rarely, if ever, correspond to any simple periodic function. Thus, a pragmatic approach is to recognize and accommodate the consequences of undersampling and live with what is possible.

A good rule of thumb for ensuring accurate spectral characterization is the "three data point" rule. If a single fluorophore is present, there should be at least a three-WDP spread across the FWHM of the emission. If multiple fluorophores are present, then three WDPs should be used to define the difference between wavelength maxima or profile separation of the two spectra. For example, if a single fluorophore has a FWHM of 75 nm, then a WSI of 25 nm will accurately characterize the FWHM of the profile. If two 75-nm FWHM spectra are collocated and the profiles are separated by ~20 nm, then we need a WSI smaller than 7 nm to define the true combined spectral profile. When multiple fluorescence emissions are present, larger numbers of WDPs and smaller WSIs are needed.

Simply put, aliasing in a CSI system is responsible for the inaccurate characterization of a natural spectrum due to undersampling of the natural spectral emission. Insofar as there is no limit to the degree of undersampling, there is also no limit to the degree of aliasing and inaccurate spectral characterizations. Aliasing is a systematic instrumental error that is an inherent property of an instrument that cannot be corrected by optomechanical adjustment such as refocusing or realignment.

Aliasing can be responsible for deformities in a spectral profile that are often unrecognized and frequently ignored simply because they are reproducible and precise. However, aliasing can adversely affect PVR, WTWR, and FWHM values and wavelength accuracy. Ironically, aliasing gives a researcher the opportunity to be precisely and reproducibly wrong.

Aliasing can produce multiple, predictable manifestations of a spectrum, each of which is individually referred to as an "alias." The challenge is to differentiate between aliasing, which is inherent, and instrumental errors such as wavelength inaccuracy or defocus that are likely to be caused by misalignment that can be corrected by a technician. The following section describes the determination of theoretical alias profiles that can be compared with observed profiles by using the MIDL as a standard spectral source. The object of these benchmark tests is to enable researchers to compare the performance of one instrument with that of another and to characterize instrument stability. Standardization enables us to identify errors and confirm the validity of a series of acquisitions.

Expected Aliases With a 5-nm WSI

Any instrument that takes spectral data with a WSI of 1 nm will reproduce the profile shown in Figure 1b and will be free of aliasing. The MIDL spectrum is a "fingerprint" that can be used as a reference spectrum. When this spectrum is acquired with a WSI larger than 1 nm, by definition it will be undersampled and the spectral profile will be an inaccurate representation of the original, in other words an alias.

Construction of Derived Reference Spectra

The first task in the process of comparing observed with theoretical spectral profiles is to predict the aliases

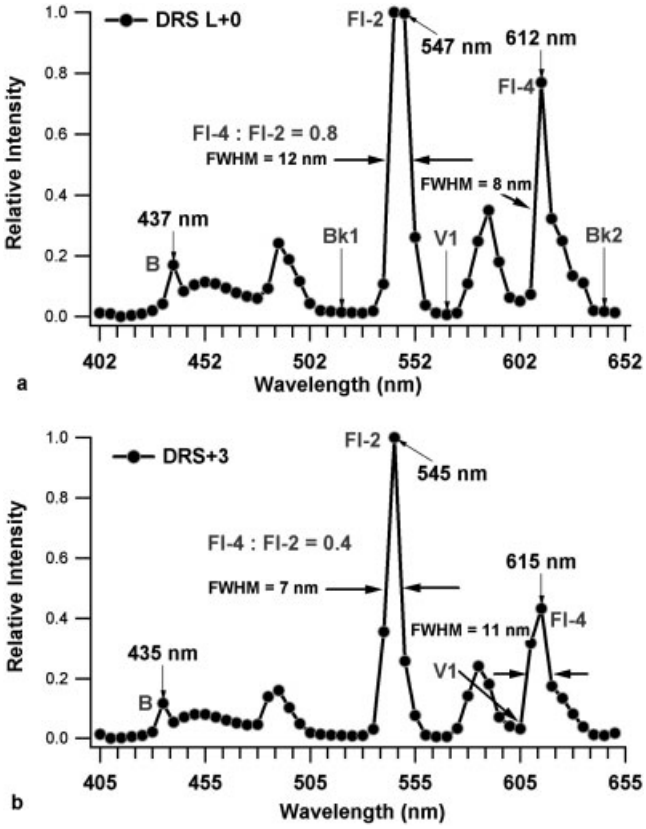

FIG. 2. By using a WSI of 5 nm, consistent with LCSI systems, spectra were mathematically simulated to produce derived reference spectra (DRS), illustrating the expected spectral profiles for two predictable aliases with starting wavelengths 3 nm apart: (**a**) L + 0 and (**b**) L = 3. The Fl-2 feature is bisected by two WDPs (a) or one WDP (b). In this case, the alias changes the wavelength ratio between Fl-2 and Fl-4, when measured at the peak maxima and the FWHM of all spectral features.

that can be expected in a CSI system. If the WSI of the instrument is 5 nm, then aliasing can be observed and quantified by acquiring two spectra, one taken with a starting wavelength 2 or 3 nm shifted from the other. The resultant spectra will present two different spectral profiles or aliases. For example, if we acquire one spectrum of an emitting source from 400 to 700 nm and another starting from 403 nm to 703 nm, they will be the same when aliasing is absent but different when aliasing is present.

Given the narrow spectral features of the MIDL, we expect that LCSI and ZCSI systems with WSI values of 5 and 11 nm, respectively, would produce aliased spectral profiles, and we would expect that two spectra each acquired with a wavelength offset would present different spectral profiles of the MIDL emission.

To calculate the theoretical profiles of these aliases, we compute derived reference spectra (DRS) based on an ASCII dataset for the spectrum shown in Figure 1b. In this example, we calculate two aliases that we expect to be present in an LCSI system with a WSI of 5 nm. The first task is to simulate an LCSI wavelength scan, starting at a nominal 0 wavelength point, and then to calculate the spectral profile that would correspond to alias DRS L + 0. The second simulated wavelength scan would start with a wavelength offset of 3 nm and produce alias DRS L + 3. Later we will acquire two real spectra on a LCSI system under similar conditions and compare them with the two DRS aliases.

To derive each DRS spectrum, we export the 1-nm WSI ASCII data from the MIDL test certificate into Excel, and we sum the intensity values over sequential 5-nm increments (for a WSI of 5 nm) for the full spectral range starting from 400 nm for DRS L + 0. For example, the first alias data point is derived by summing MIDL data points a1 + a2 + a3 + a4 + a5 = A1, the second alias data point by summing data points a6 + a7 + a8 + a9 + a10 = A2, and so on. Repeat the calculation with an offset of 3 nm for a start at 403 nm for DRS L + 3. The simulated scans can then be plotted. These simulations are the predicted spectral aliases. With this approach, we can construct all five DRS (aliases) for integer values by changing the wavelength offset incrementally for all five aliases.

The resultant DRS are shown in Figures 2a and 2b, with the SCF parameters listed in Table 3. The wavelength values on the abscissa of Figures 2a and 2b start at ~402 and ~405 nm, respectively, because the LCSI system reports raw data at the start wavelength (400 nm) plus 50% of the WSI. Hence, for a 400-nm start and 5-nm WSI, the first data point will appear at ~402 nm, and ~405 nm for a 403-nm start.

Aliases that correspond to noninteger wavelength offset starting points will result in profiles in which WTWR, PVR, and FWHM values differ. It is understood that most researchers tend to start and finish at given wavelengths, but optomechanical instability can cause wavelength shifts. The profiles shown in Figures 2a and 2b can now be used to predict the spectral profiles that can be expected from an LCSI system that is in perfect optomechanical condition.

Because the alias can be chosen by offsetting the starting wavelength, all CSI systems of the same type or model can be standardized to produce any given alias. This standardization would ensure that the same findings would be observed for the same experiment on any instrument of the same type.

Algorithms used for spectral unmixing rely on accurate, reproducible spectral data that can be used as training sets to enable spectral mixtures to be separated, or unmixed, into their components. If a spectrum shifts due to changes in pH, binding, optomechanical malfunction, or wave-

Table 3
Spectral Characterization Functions of Two Selected Aliases for WSI of 5 nm

	WTWR	PVR	FWHM (F1-2)	FWHM (F1-4)
DRS L + 0	0.8	22	12	8
DRS L + 3	0.4	19	7	11

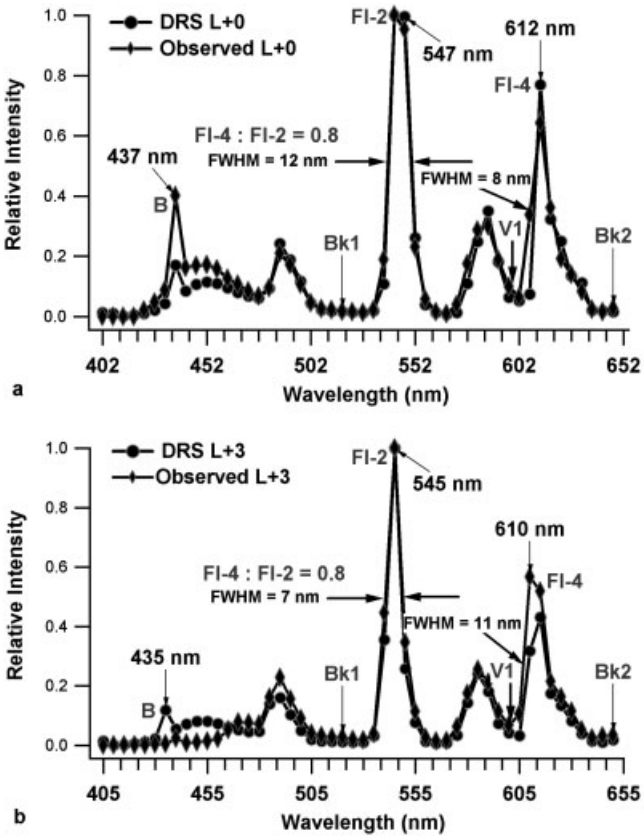

FIG. 3. Observed spectra from system L1 superimposed onto computed DRS for (**a**) L + 0 and (**b**) L + 3. The observed spectra fit well with the DRS simulations. Note how the FWHM and the ratio between spectral features at Fl-2 and Fl-4 have changed between the two aliases.

length offset, the robustness of an optimized algorithm could and probably will be compromised. Therefore, it is essential that changes that may occur to a spectrum in a real-life sample be recognized and accommodated. The consequence of undersampling (aliasing) may be that errors go unrecognized.

EXPERIMENTAL CHARACTERIZATION OF LCSI SYSTEMS

LCSI systems use a spectrometer that produces wavelength-dispersed light that is incident on one or more slit assembly that translates across the spectral dispersion plane (SDP), each associated with a PMT. There may be three or four such slit/PMT assemblies. For simplicity, when we use the term "PMT 1" (2 or 3), we refer to the spectral output of the entire slit/PMT assembly.

LCSI systems generate a spectral scan (lambda scan) by using any of up to four PMTs. Each PMT is associated with its own exit slit assembly that is located on the SDP of the spectrometer. The spectral profile of an emission source should be the same for all the PMT assemblies in the system after accounting for the QE of each.

System L1: Calibration and Validation

Observed versus theoretical DRS profiles. By following the setup used to generate the DRS, the Leica TCS-SP1 located at the USEPA (system L1) was used to acquire two 50-WDP scans, one starting at 400 nm (observed L + 0) and the other at 403 nm (observed L + 3), by using the output from PMT 2. The WSI was set at 5 nm (recall that the values on the abscissa of all Leica graphs that start at ~402 and ~405 nm reflect actual start wavelengths of 400 and 403 nm).

The spectral data was then digitized, exported to Excel, and overlaid with the appropriate DRS (Figs. 3a and 3b). The LCSI data are indicated with triangles and the DRS with circles. Note that there is a very good fit between the experimentally acquired data and the theoretical DRS. We observe that, as expected from the DRS, the spectral profiles of the observed L + 0 and L + 3 differ and are close enough to theoretical predictions to be within experimental accuracy. Given that these results are within expectations, no realignment or refocusing is called for due to the differences between these spectral profiles. We also observed that there was very little signal at wavelengths shorter than 460 nm and no trace of the 436-nm Hg emission line (B) in Figure 1b. The SCF values for the observed versus DRS values for PMT 2 are listed in Table 4. We observed that the output of PMT 2 was deficient in the blue region of the spectrum. The QE of the PMT should have been adequate to record the 436-nm Hg line in the MIDL; this was reason enough to request a Leica service call.

Note that the FWHM of the spectral features at Fl-2 and Fl-4 for alias L + 0 are 12 nm and 8 nm, respectively. However, for alias L + 3, these values are reversed. This confirms that the starting wavelength of a scan has a significant effect on the profile of the spectrum, as the DRS profiles predicted. As expected from the DRS profiles, the nominal WSI of 5 nm does not translate into a spectral resolution of 5 nm determined by measuring the FWHM of the emission features.

The WTWR peak intensity ratio, measured at peak intensity, between F-2 and Fl-4 also changes from one alias to another; the peak ratio of Fl-4 to Fl-2 for observed L + 0 is 0.8, but for DRS, the observed L + 3 it is 0.4. Failure to recognize this possibility could have a serious effect on the accuracy of wavelength ratio measurements in a real-life sample.

This experiment clearly demonstrates that, if a wavelength shift occurs due to a deliberate change in starting

Table 4
Spectral Characterization Functions of Expected Aliases Versus Observed Data From System LI (PMT 2)

	WTWR	PVR	FWHM (F1-2)	FWHM (F1-4)
PMT 2 observed L + 0	0.8	17	12	10
DRS L + 0 theoretical	0.8	22	12	8
PMT 2 observed L + 3	0.6	13	9	13
DRS L + 3 theoretical	0.4	19	7	17

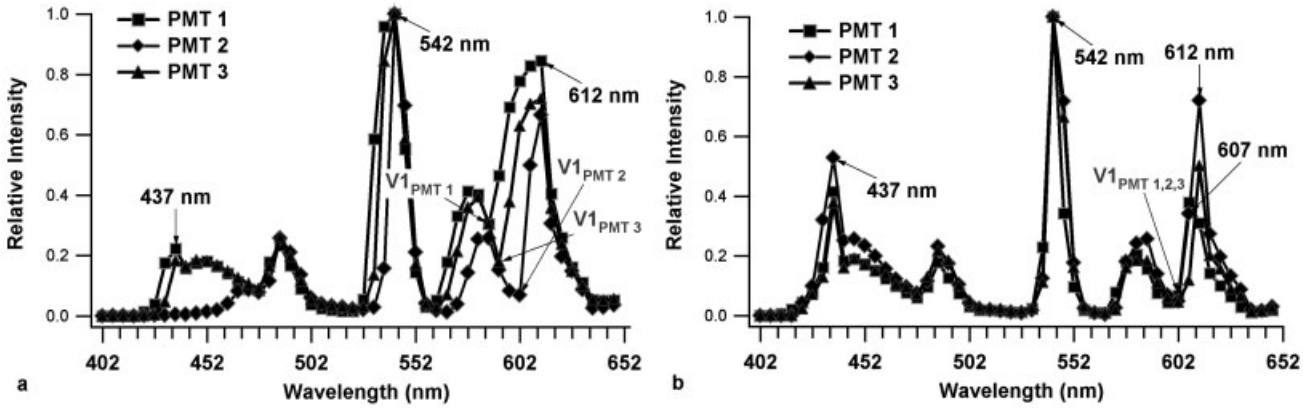

FIG. 4. The same MIDL spectrum as presented by all three PMT assemblies in system L1. **a:** The three profiles differ widely in FWHM, contrast, and ultraviolet signal intensity. PMT 2 fits L + 0, whereas PMTs 1 and 3 fail to match any predictable alias; thus, the errors suggest optomechanical inconsistency. **b:** After optomechanical realignment, the three profiles are consistent (no PMT was changed).

wavelength or because of an unsuspected optomechanical error, wavelength ratios can shift significantly. This could challenge the identification and characterization of real changes in a spectral profile due to localized changes in pH, ionization, binding, or physiology.

Comparison of results for PMTs 1, 2, and 3. This protocol was repeated for PMT 1 and 3 assemblies. Figure 4a shows an overlay of the scans presented by PMTs 1, 2 and 3. We expected that the three profiles would superimpose. They did not, even if we allow for differences in the QEs of the PMTs.

The wavelengths of the peak maxima of the spectral features shown in Figure 4a are within expectations, given a WSI of 5 nm. This indicates that the three PMTs share a common optical axis. Before readjustment, PMT 1 was the only PMT that presented a resolved feature at 436 nm, indicating that its QE is superior to those of the other PMTs or that the optomechanical parts that serve it are in better physical placement. However, the spectra from PMTs 1 and 3 also present significantly broader, less well-defined peaks and valleys, suggestive of spectral defocus and possible misalignment. Given the poor correlation across the outputs of the three PMTs, the Leica technician was called in to resolve the deficient blue response of PMT 2 and to readjust the assemblies leading to PMTs 1 and 3. While waiting for a service technician, we used only PMT 2 for acquisitions above 470 nm because this was the closest match to theoretical predictions.

Performance after system readjustment. After the Leica technician replaced all the slit sliders in the system, there was significant improvement; however, the PMTs were still not performing equivalently. The before and after SCF values are listed in Table 5. After adjustment, the PVR value for PMT 1 improved from 2 to 11 and that of PMT 3 improved from 5 to 15. This significant improvement coincided with an improvement in FWHM from larger than 25 nm down to 10 nm for PMT 1 and from larger than 25 nm down to 7 nm for PMT 3 at the 611-nm peak.

All PMTs now present adequate blue efficiency around 436 nm (Fig. 4b). No PMT was exchanged. This indicates that the problem of attenuation in the blue response was a function of optomechanical placement errors. We also note that the profile (alias) of the spectrum for PMT 1 before adjustment correlated with DRS L + 0 (for a 400-nm start); however, after adjustment, the profile was very close to DRS L + 3. This is a good example of how mechanical issues can present unexpected changes in performance. It suggests that routinely checking the spectral profiles generated by the system can alert the user to changes before they affect the interpretation of the results of an experiment.

How to eliminate aliasing in an LCSI. We know that aliasing is a problem of undersampling a natural spectrum; hence, increasing the sampling frequency should decrease or eliminate aliasing. The Leica software enables lambda

Table 5
Spectral Characterization Functions Before and After Readjustment of System L1

	WTWR		PVR		FWHM (F1-2)		FWHM (F1-4)	
	Before	After	Before	After	Before	After	Before	After
PMT 1	0.8	0.4	2	11	17	7	>25	10
PMT 2	0.7	0.7	15	23	13	10	13	9
PMT 3	0.7	0.5	5	16	14	9	>25	7
DRS L (0/+3)	0.8/0.4		22/19		12/7		8/11	

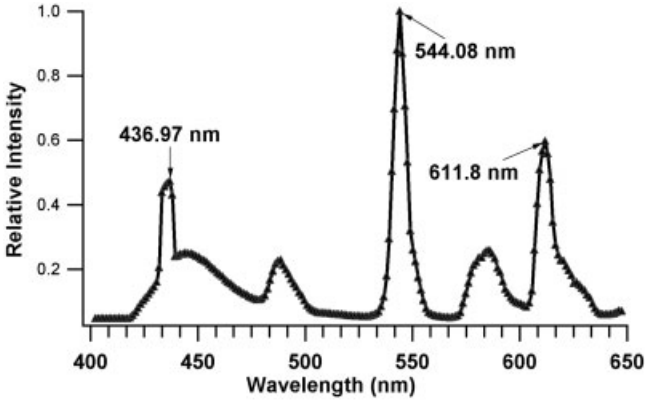

FIG. 5. Aliasing can be decreased or eliminated by increasing the number of WDPs. This MIDL spectrum was acquired with 200 WDPs on an LCSI system. The spectrum was sampled in 1.23-nm steps, each with a WSI of 5 nm. The bandpass of the spectral features present a constant FWHM value of ~7 nm. This demonstrates that the WSI value limits but does not determine spectral bandpass. However, the number of WDPs does determine the degree of aliasing.

scans to be acquired with each acquisition 1.25 nm apart while maintaining the same WSI of 5 nm.

A lambda scan of the MIDL was generated with 200 acquisitions between 400 and 650 nm (Fig. 5). We can see from Table 6 that the 200-WDP scan presents FWHM values that are now equivalent to the narrowest that can be observed with for L + 0 or L + 3. Given that wavelength dispersion (the physical distance between two wavelengths 1 nm apart) is greatest in the blue, the FWHM of the 436-nm Hg emission (line B in Fig. 1b) should be narrower than that of the 545-nm emission (equation 1, which is discussed in greater detail in the Appendix). However, the FWHM at 436 nm is the same ar ~7 nm as it is at 545 nm, suggesting that ~7 nm may be close to the limiting spectral bandpass of the system.

These results indicate that aliasing has been greatly decreased, to the point that the spectral profile of the MIDL tends toward that generated by the PARISS system.

The wavelength accuracy has also increased to the point that the error between actual and acquired values is smaller than 1 nm over the entire range of 400 to 650 nm.

The downside to generating such a high-density WDP lambda scan is that it is very slow due to the sequential nature of the wavelength acquisition. Many fluorescent samples would photobleach before completion of a scan. This is a good illustration of how the WSI determines the bandpass or spectral resolution and how the number of WDPs determines accuracy and minimizes aliasing.

Discussion and conclusions. The MIDL was shown to be an excellent diagnostic tool that clearly identified inconsistencies and errors in accuracy and aliasing. The ability to identify aliases can be a powerful tool for optimizing an experimental setup. For example, if a fluorophore emits ~545 nm, then for this instrument alias L + 3 would provide spectral FWHM resolution (7 nm) superior to, e.g., L + 0 where the FWHM would be 12 nm. To acquire a spectrum for L + 3, a scan should be started at 403 nm (or, by extension, 503 nm). If the fluorophore emits ~612 nm, then the scan should start at 545 nm to provide alias L + 0. In these examples, the spectral bandpass will be optimal at these wavelengths. Evaluation of the profiles of the other aliases (use DRS L + 1 through L + 4) would allow us to determine the appropriate start wavelengths for alternative spectral ranges. In a real experiment, a third-party researcher with the same instrument model could match the alias to reproduce the same spectral profiles.

In this report, we only show the aliases for DRS L + 1 and L + 3; however, it is easy to construct the DRS profiles for L + 1, L + 2, and L + 4. All aliases are equally predictable and reproducible and can be observed if the starting wavelengths are shifted to 401, 402, and 404 nm, respectively. This is an excellent way to demonstrate that the instrument imposes artifacts onto the natural spectrum of an emitting object that cannot be "cured" by a technician.

Calibration at wavelengths longer than 650 nm. A 1-inch-diameter, 766-nm, 10-nm BPF was placed on a standard blank 1- × 3-inch microscopic slide located over the objective of our inverted LSCI system L1. The filter was top illuminated with a halogen lamp. A scan was acquired from 693 to 783 nm in 20-WDP acquisitions, each with a WSI of 5 nm.

PMT 1 was unable to scan the red region, so we show the results for PMT 2 and 3 in Figure 6, after readjustment of the system. PMT 2 placed the peak maximum at 748 nm with an FWHM of 39 nm, and PMT 3 presented a profile with a center wavelength of ~768 nm and an FWHM of 22 nm. Only PMT 3 was accurate within the WSI of 5 nm. It is apparent that accuracy and consistency over the entire wavelength range of 400 to 800 nm continue to be a challenge for this instrument.

Dielectric filters are designed for use in collimated light; however, in this instance, the filter was used in focused light. As a consequence, we did not expect the absolute peak wavelength and bandwidth to conform to the certificate, but the conformation was suitable for making *relative* comparisons of one PMT with another.

Effect of Spectral Inconsistency on Real-Life Studies

BFP slide. To confirm the findings observed with the MIDL with a more familiar tool, we characterized a BFP test slide using system L1 (we used the BFP made by

Table 6
Comparison of Spectral Characterization Functions of PARISS Versus CSI Systems With Various Numbers of WDP

	WTWR	PVR	FWHM (F1-2)	FWHM (F1-4)	FWHM (B 436)
PARISS MIDL	0.7	35	6	4	1
200 WDP	0.6	22	7	8	7
50 WDP (DRS L + 0)	0.8	22	12	8	N/A
50 WDP (DRS L + 3)	0.4	19	7	11	N/A

N/A, not available.

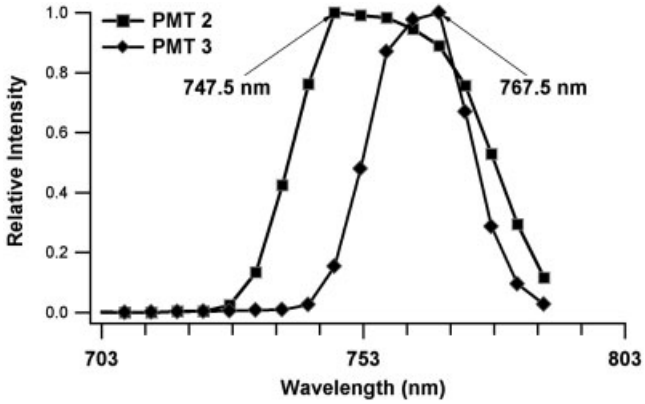

FIG. 6. Spectral scan of a 10-nm BPF centered at 766 nm through PMTs 2 and 3 acquired with a Leica TCS-SP1 (PMT 1 was unable to scan over this wavelength range). The FWHM for PMT 2 is 39 nm and that for PMT 3 is 22 nm, and each peaks at different wavelength maxima. This suggests that the mechanical alignment of the two slit assemblies is different in these two cases, with PMT 2 presenting the larger error.

Applied Precision Inc., but the BFP produced by Chroma Corporation works equally well).

This BFP material nominally excites at 408 nm and has an emission peak at 440 nm. In this test, we excited with the 365-nm laser line and still obtained adequate fluorescence signal to enable relative tests between PMTs. Figures 7a and 7b show the spectral characterizations before and after the system was readjusted. Before readjustment of system L1, PMT 1 provided coverage over most, but not all, of the emission range of the blue plastic (Fig. 7a). However, PMT 3 loses signal up to ~438 nm, thereby cutting off about half the emission signal, whereas PMT 2 only cuts at ~472 nm. After readjustment, all PMTs produced good blue coverage (Fig. 7b) and consistent spectral profiles; however, PMT 3 presented a noisy line profile. These results are consistent with the characterizations obtained with the MIDL.

Analysis of sperm. Spectral scans of the sperm samples were acquired at 400 to 650 nm (also shown as starting at 402 nm on the plots in Figs. 8a and 8b).

As expected, before the instrument was readjusted, PMT 2 displayed a loss of light below 472 nm, making PMT 2 unusable for this experiment (Fig. 8a). Given the poor spectral resolution of PMTs 1 and 3 (established with the MIDL and confirmed with the BFP), the precision and accuracy of all sperm characterizations acquired through any of the three PMTs are in question at this time.

After readjustment, the scans were repeated, and results are shown in Figure 8b. As expected, the blue light throughput has improved for PMT 2 and the spectral profiles of DAPI though all PMTs are now consistent. However, PMT 3 presents a noisy spectral profile, with jagged edges on the trailing side of the spectrum. The peak fluorescence for DAPI-stained sperm nuclei is reported to be 460 nm, although the instrument reported a peak wavelength of 437 nm. We can only speculate as to the cause for this shift; however, because the MIDL reported good wavelength accuracy, we tend to believe that the observed wavelength of the DAPI signal was accurate. This highlights the limitations of using biological samples for testing instrumental accuracy.

Conclusion. Given the supporting experimental results from the BFP, sperm acquisitions, and 766-nm BPF, it is clear that the MIDL is effective at predicting performance in real-life applications.

System L2: Characterization of an LCSI With an Acousto Optic Beam Splitter

This model is also manufactured by Leica and is more advanced than the LCSI TCS-SP1 system L1 at the USEPA. It uses an Acousto optic beam splitter rather than dielectric mirrors. Figure 9a shows an inconsistency across the three PMT assemblies in a manner analogous to those errors found in system L1. WTWR and PVR values were poor, with inconsistent FWHM values (Table 7). Comparison of the observed peak maxima with the true wavelength maxima listed in Table 1 show that wavelength accuracy was less than should be expected for a WSI of 5

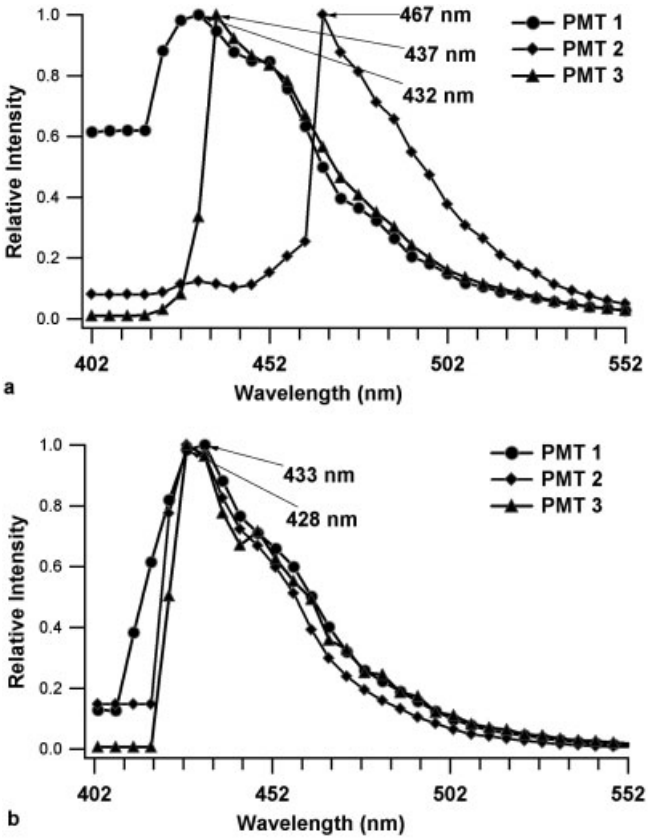

FIG. 7. Characterization of a blue plastic slide excited at 365 nm (**a**) before and (**b**) after system realignment. Based on the differences shown in Figures 4a and 4b, these results were expected. In both cases, blue/ultraviolet intensity was decreased before system readjustment and improved after adjustment. This demonstrates that the MIDL offers a fast means of determining spectral consistency and wavelength coverage.

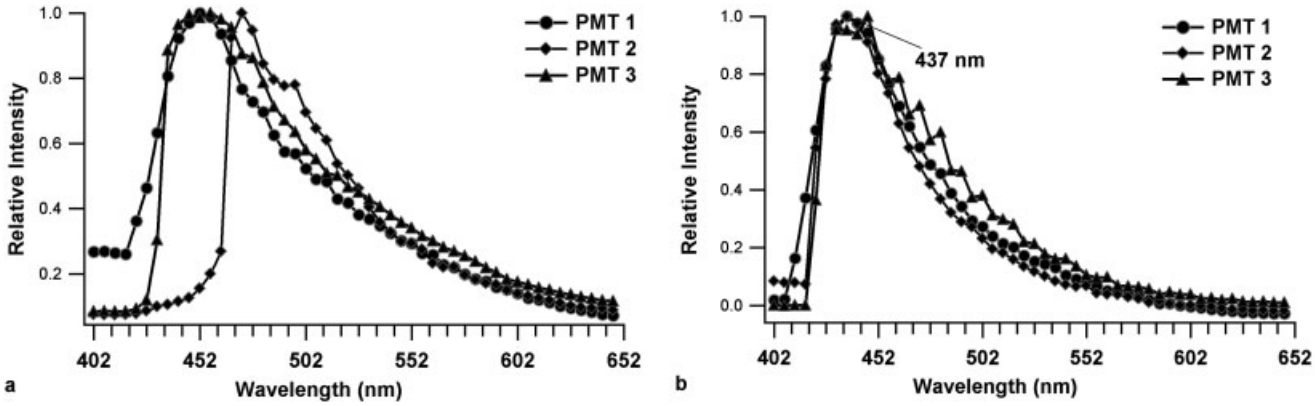

FIG. 8. The effect of spectral errors on a real-life sample was studied with DAPI-stained sperm (**a**) before and (**b**) after system realignment. The improvement in results was remarkable. The poor results observed in panel a demonstrate the need to confirm that a system is in good optical condition before drawing conclusions.

nm. Given these findings, a Leica technician realigned the entire system. The result then showed much improved performance (Fig. 9b and Table 7). After realignment, each PMT profile shifted from alias DRS L + 3 to alias DRS L + 0, thus reinforcing and confirming that optomechanical errors can affect the profile of a spectrum. It also suggests that wavelength ratios obtained in a real experiment may change after realignment. Moreover, when comparing results with colleagues with similar instruments, the alias has to be known before comparisons can be made.

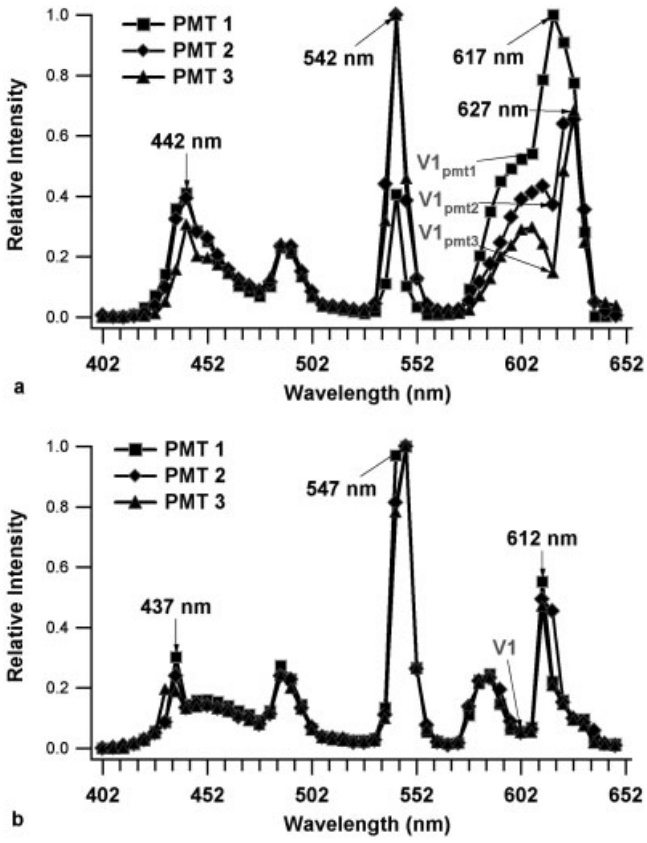

FIG. 9. System L2 (TCS-SP2, AOBS; **a**) before and (**b**) after realignment. The MIDL clearly identified the inconsistencies (a) that were corrected (b). The aliases shown in panel a were a good fit to L + 3 but changed to L + 0 after realignment. This could result in wavelength ratios obtained before adjustment that changed after adjustment and indicates that relative and absolute measurements can be compromised.

System L3

System L3 is a Leica TCS-SP1 identical to system L1. As before, two lambda scans were generated, one starting at 400 nm and the other at 403 nm (Figs. 10a and 10b). We observed that all three PMTs were consistent from 477 to 650 nm (Fig. 10a). However, only PMT 1 presented a clear indication of the 436-nm Hg line. PMT 3 presented very poor light throughput below 477 nm. After the aliasing test, PMT 2 was observed to be inconsistent to the point that it was barely useable at this wavelength starting point (Fig. 10b). The overall performance was consistent with that found in system L1.

From Table 8, we note that none of the spectral profiles was a good fit with DRS L + 0; however, they were close to DRS L + 3 and L + 4 (not shown). This suggests that the actual starting wavelength was more likely to be closer to 401 nm than to 402 nm. Perhaps there was a ~1 nm error at 403 nm that was not evident given the WSI of 5 nm. The imperfect fit to DRS L + 0 could well have been due to an optomechanical error that resulted in a subnanometer wavelength offset or an error in the value of the WSI. Nevertheless, the wavelength accuracy of the MIDL features was within the WSI of 5 nm. This is another good example of the ease with which the MIDL can be used to diagnose errors and inconsistencies in the performance of the system.

Table 9 presents a comparison of the performance of the three LCSI systems tested after realignment whenever applicable. Even though repeatability was good for all three systems, we were unable to obtain two identical

Table 7
Spectral Characterization Functions of System L2

	WTWR		PVR		FWHM (F1-2)		FWHM (F1-4)	
	Before	After	Before	After	Before	After	Before	After
PMT 1	3	0.6	2	13	7	11	>25	7
PMT 2	0.6	0.5	2	13	7	11	15	11
PMT 3	0.5	0.5	4	11	7	11	15	7
DRS L + 0	0.8		22		12		8	
DRS L + 3	0.4		19		7		11	

MIDL spectral characterizations between either two PMT assemblies within the same system or with unrelated systems.

Effect of Pinhole Diameter on Bandpass in Leica Systems

In this section, we determine the effect of changing the physical size of the pinhole on the spectral capabilities of the instrument. In a classic confocal microscope, the researcher chooses the size of the pinhole that is normalized to Airy disk units. Decreasing the pinhole size increases contrast and spatial resolution in the FOV but limits the amount of light passing through the system and, ultimately, the S/N ratio. It is not uncommon for researchers to use pinhole sizes in excess of the size of the Airy disk. It is equally not uncommon to change the objective from low power to high power. In each of these cases, there is an effect not only on spatial resolution and light throughput (see Light Throughput Equation in the Appendix) but also on spectral resolution and bandpass.

Briefly, a CSI system images a point in the FOV through a matched pinhole that is also the entrance aperture to a spectrometer. From equations 1 and 2 (discussed in detail in Spectrometer Operating Characteristics in the Appendix), we know that increasing the width of an aperture (in this case, the pinhole) can degrade the observed bandpass (BP_{net}) as measured by the FWHM of a spectral feature. For monochromatic light, or the emission of the MIDL, the terms that determine bandpass for a gaussian profile are given in equation 1.

$$BP_{sw} = Disp \times W_{epa} \quad (1)$$

For an extended emission such as a fluorophore, the net bandpass is determined with equation 2.

$$BP_{net} = SQRT(BP_{nat}^2 + BP_{res}^2 + BP_{sw}^2) \quad (2)$$

where

- BP_{sw} (nm/mm) is the bandpass determined by the width of the entrance aperture, W_{epa}, for the wavelength dispersion at a particular wavelength. In this case, it is calculated by measuring the FWHM of a monochromatic spectral feature emitted by a light source.
- Disp (nm/mm) is the physical distance that separates two wavelengths. In a diffraction grating-based system, this value is constant regardless of wavelength; however, Disp changes with wavelength in a prism-based system.
- W_{epa} (mm) is the *greater* of the width of the exit aperture or the image of the entrance aperture (in a CSI system, the entrance aperture will be the pinhole). The exit slit in an LCSI system will typically define the W_{epa}.

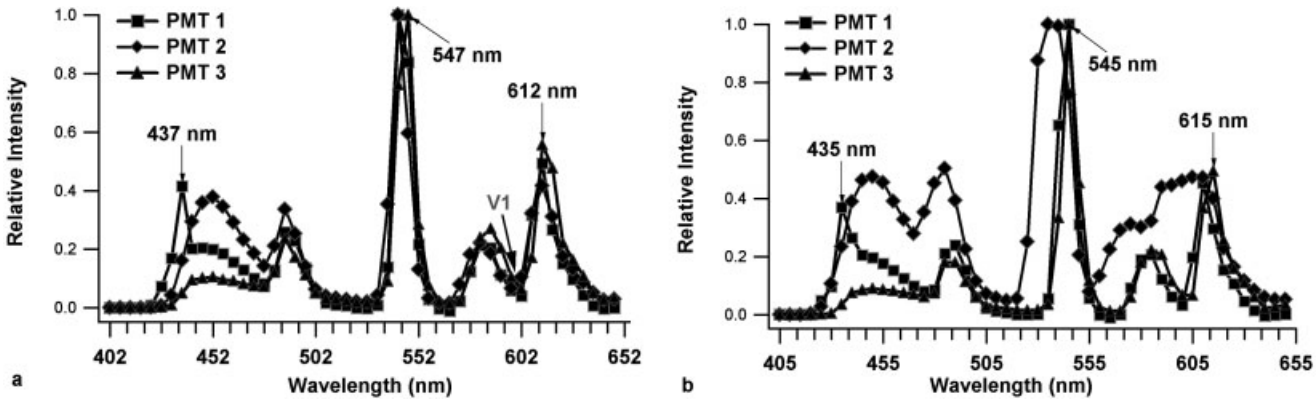

FIG. 10. **a, b:** The two aliases of system L3 are a better fit to aliases L + 3 and L + 4, suggesting errors in wavelength accuracy. The MIDL test alerted us to the erratic performance of PMT 2 between panels a and b. Even though the scan shown in panel b started at a wavelength 3 nm higher than that shown in panel a, the wavelength maxima of the spectral features appeared at shorter wavelengths.

Table 8
Spectral Characterization Functions of System L3 Versus Aliases DRS + 3 and + 4

	WTWR		PVR		FWHM F1-2		FWHM F1-4	
Alias	402	405	402	405	402	405	402	405
PMT 1	0.5	0.5	11	13	11	11	13	15
PMT 2	0.4	0.5	10	2	10	>20	17	N/A
PMT 3	0.5	0.5	14	11	11	8	14	15
DRS (+3/+4)	0.4	0.5	19	15	7	10	11	11

N/A, not available.

BP_{net} is the net delivered spectral bandpass.
BP_{nat} is the natural bandpass of the emission line.
BP_{res} is the limiting resolution of the spectrometer.

Because the size of the pinhole is typically matched to the size of the Airy disk, spectral resolution will degrade as spatial resolution increases, counterintuitive though this may be. To understand why, see Effect of Pinhole Illumination on Bandpass in the Appendix.

The effective size of the pinhole depends on whether it is uniformly filled. An extended source such as the MIDL always uniformly fills the pinhole regardless of the pinhole diameter. A point source, such as an Airy disk, may only partly fill an oversized pinhole. We observed, however, that the distinction between the degree that a point (Airy disk) and an extended source actually illuminate a pinhole is less than obvious. Tests showed that, as a pinhole is opened in pure laser confocal mode, there is an increase in the illuminated area of the pinhole that tends more to that of an extended source than expected, even for weakly scattering samples. The experimental work is described in Light Throughput Equation of the Appendix. It is evident that, even though a relation between the bandpass and the pinhole size was observed with a MIDL light source, in many cases the same or similar relations will apply, even in a point confocal mode.

To determine the agreement between theoretical and observed spectral bandpass values as the pinhole diameter increases, for a WSI of 5 nm, we ran a wavelength scans using an LCSI TCS-SP1 between 520 and 580 nm at the pinhole diameters listed in Table 10. Figure 11a shows an overlay of the spectral scans for pinholes 1, 4, and 7 for alias L + 0 and Figure 11b shows an overlay for alias L + 3.

Determination of Theoretical FWHM Values

For a real-life experiment with light that is polychromatic in a system with a given bandpass, we use equation 2 to determine the theoretical BP_{net}. First, however, we need values for the terms W_{epa}, BP_{nat}, BP_{res}, BP_{sw}, and wavelength dispersion (Disp).

W_{epa}: We take the actual size of the pinhole with the initial assumption that the image of the entrance pinhole is matched to the width of the exit slit. If the width of the slit is not matched to the width of the image of the pinhole, this will become apparent when we correlate theory with observation.

BP_{nat}: The emission band centered at 545 nm is a composite of the 546-nm Hg line (which is essentially monochromatic) and an inorganic fluorophore peaking at 545 nm; the composite FWHM is 2 nm (computed from PARISS data and by iteration).

BP_{res}: Using basic optical principles for a flint glass prism spectrometer and focusing optics consistent with the size of the Leica spectrometer box, we expect a limiting resolution between 4 and 7 nm. We iterated the terms BP_{res} and BP_{sw} in equation 2 to determine that that the closest fit for BP_{res} is 6 nm. We also recall that, when we acquired the 200-WDP scan, the observed bandpass (BP_{net}) was a constant 7 nm at 436 nm and 545 nm, indicating that our estimate was close to optimum, given that BP_{res} will always be less than BP_{net}.

Disp: Leica does not supply this information; therefore, the dispersion value was also calculated by iterating until the theoretical BP_{net} corresponded to the observed BP_{net}. The calculated value that produced the closest fit was 26 nm/mm at 545 nm.

BP_{sw}: This is calculated from equation 1 by multiplying the deduced Disp by the pinhole size (W_{epa}).

Comparison Between Theoretical and Observed Bandpass

Three plots are shown in Figure 12 for the theoretical versus observed bandpass including (a) the theoretical BP_{net} for each pinhole size, (b) the observed BP_{net} for alias L + 0, and (c) the observed BP_{net} for alias L + 3. All values of FWHM were measured at the 545-nm MIDL line. By

Table 9
Comparison of All LCSI Systems Tested After Readjustment

	WTWR			PVR		
System	PMT 1	PMT 2	PMT 3	PMT 1	PMT 2	PMT 3
L1	0.4	0.7	0.5	11	23	16
L2	0.6	0.5	0.5	13	13	11
L3	0.5	0.5	0.5	11	10	14

Table 10
Pinhole Diameter Versus Airy Pinhole Number for a Leica 10× Objective, Plan Apochromatic, 0.4 NA

Pinhole no.	1	2	3	4	5	6	7
Diameter (μm)	80	156	241	319	397	475	558

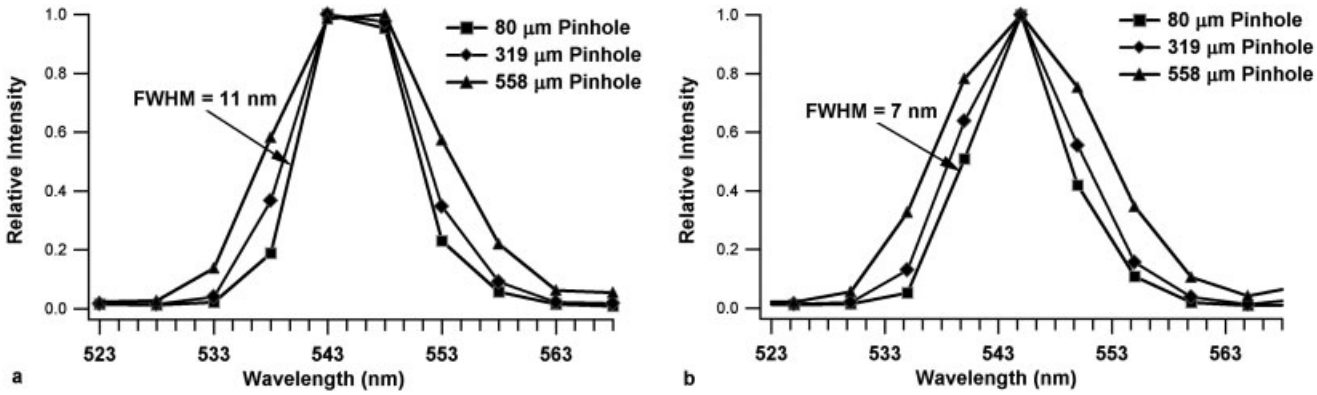

FIG. 11. Pinhole diameter versus bandpass (FWHM) on LCSI systems. By using the MIDL as a light source, the FWHM of the 545-nm spectral feature increases nonlinearly but predictably as the pinhole diameter increases. In this case, the FWHM at 545 nm is broader for alias L + 0 (**a**) than for L + 3 (**b**). Most of the energy at 545 nm is centered in a single WDP for L + 3 and is therefore more sensitive to changes in FWHM as a function of pinhole diameter.

using 6 nm for BP_{res} and 26 nm/mm for the wavelength dispersion at 545 nm, we obtain an almost perfect fit with the observed FWHM values for alias L + 3, which degrades more or less linearly with pinhole diameter. The excellence of the fit with the theoretical FWHM indicates that the width of the exit slit is always matched to the size of the pinhole or that the image of the pinhole is always larger than the effective width of the slit. Of the two options, the latter is more likely. It also means that, if the image of the pinhole is larger than the width of the slit, then some useful signal is lost on the slit jaws. Note that the FWHM for alias L + 3 for an Airy disk of 1 (pinhole diameter ~80 μm) is ~7 nm and confirms that the WSI of 5 nm limits, but does not determine or equal, the observed bandpass of the system.

The FWHM curve for alias L + 0 is more complicated because the peak of the spectral feature at 545 nm is captured by two WDPs in an uneven split and degrades nonlinearly with an increase in pinhole diameter. The limiting resolution was observed to degrade by up to a factor of 2. When we substitute a value of 9 nm for BP_{res}, the fit of the theoretical to the observed FWHM values improves significantly (not shown).

Effect of Pinhole Diameter on PVR and WTWR Values

Figure 13a shows how increasing the pinhole size degrades the PVR (contrast) of the system regardless of the alias. Figure 13b shows that the WTWR values also degrade, but the magnitude of the change is highly dependent on the alias. The change in WTWR values could adversely affect ratiometric wavelength determinations and make it difficult to compare the results of experiments when using different starting wavelengths or mechanical inconsistency. Unless another instrument is used to run the same experiment with an identical setup, it could be very difficult for two researchers to correlate their findings.

Discussion and Conclusions

Observed FWHM values depend on three parameters: (a) the alias in keeping with expectations indicated in Figures 3a and 3b, (b) the pinhole diameter, and (c) the WSI. The observed spectral bandpass/resolution of the system is always worse than the WSI of 5 nm and degrades to greater than 17 nm at pinhole 7 when the pinhole diameter is 558 μm in diameter. Thus, the FWHM will degrade as the pinhole size is increased as a function of the magnification and NA of the microscope objective as described in Effect of Pinhole Illumination on Bandpass in the Appendix. A high magnification, high NA lens requires a larger pinhole than a low magnification, low NA lens. In

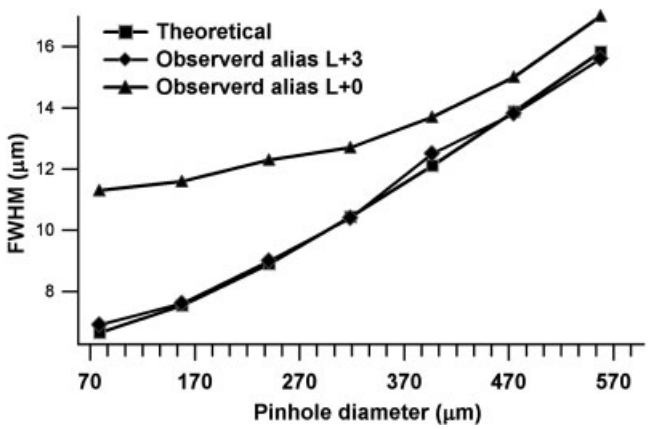

FIG. 12. Observed and theoretical plots of bandpass versus pinhole size at 545 nm (midway point between the 544-nm fluorescent maximum and the 546-nm Hg line). Agreement is almost exact for alias L + 3 because it presents the narrowest FWHM at 544 nm (single WDP). Alias L + 0 uses two WDPs to capture the full width of this line; therefore, the theoretical bandpass curve for L + 0 is not expected to agree with that for alias L + 3. Further, as pinhole size increases, the bandpass converges as the physical size of two WDPs tends to the pinhole diameter (W_{epa} is determined by the pinhole or the width of the slit, whichever is larger. When two WDPs define a single emission feature, then the slit width is effectively doubled.)

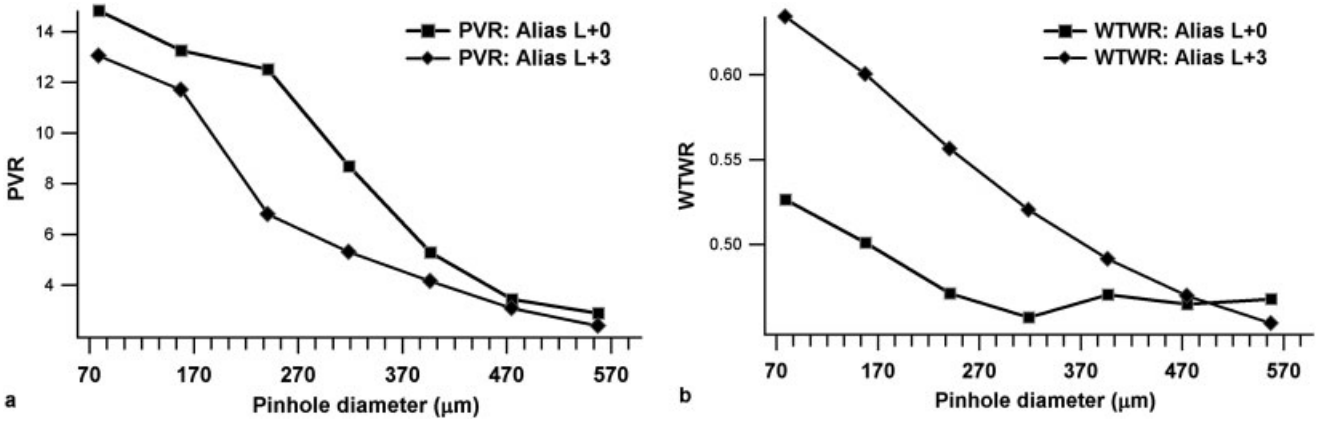

FIG. 13. PVR (**a**) and WTWR (**b**) change as a function of pinhole diameter and alias. PVR and WTWR degrade as the pinhole is opened. This should be considered when comparing data taken at 10× (small Airy disk and pinhole diameter) and at 63× (larger Airy disk and pinhole diameter).

this case, spatial resolution increases as spectral resolution degrades. Therefore, a spectral signature is dependent not only on the emission of the sample but also on the NA and magnification of the microscope objective. However, increasing the pinhole diameter from 79 μm to 158 μm (from one Airy disk to two Airy disks) results in only a 1-nm increase in bandpass rather than a factor of 2 as predicted by equation 2 due to the high limiting resolution (BP_{res} of an LCSI spectrometer ~6 nm).

This report can only skirt the subject issues that affect unmixing algorithms; however, because we observed that even weakly scattering samples tend to fill even an oversized pinhole, it is worth noting that linear unmixing algorithms are not robust in diffusing or scattering systems. Hence, any sample can be tested for scatter characteristics by using the method described in Effect of Pinhole Illumination on Bandpass in the Appendix and illustrated in Figure A2 to determine whether the Airy disk or the scatter dominates. When scatter is detected, it is appropriate to consider nonlinear algorithms to unmix commingled spectra (15).

The overall performance of each instrument and each subassembly associated with a PMT depends not only on the system being in mechanical and optical alignment but also on the alias for a given starting wavelength. We observed significant changes in wavelength ratios and PVR values as a function of aliasing as predicted by the DRS profiles. Unless aliasing is taken into consideration, it is only a matter of chance for one instrument to reproduce the findings of another. Fortunately, the alias of the instrument can be selected simply by adjusting the starting wavelength, so any instrument can be synchronized or standardized with any other. A researcher can also titrate the most appropriate alias to deliver the narrowest FWHM (highest resolution) and greatest contrast for a particular fluorophore. To ensure that the spectral profiles observed on one instrument can be reproduced on another, it would be useful if a MIDL scan were included as part of the published data for each series of experiments in addition to the objective details regarding the microscope used to acquire the data.

CHARACTERIZATION OF ZEISS CSI SYSTEMS

The ZCSI Testing Protocol

Four Zeiss LSM 510 Meta systems were selected for full testing by using the methods described for the Leica systems. However, it is not possible to change the initial starting wavelength of the spectral scan. Each scan consists of four wavelength segments of 88 nm each, and each segment acquires eight WDPs each with a WSI of ~10.7 nm. An RBF was used to characterize the region around 766 nm.

Because a ZCSI system uses a small number of WDPs (<32), we expected and observed that aliasing is significantly more noticeable with this system than with the LCSI systems. This being the case, we calculated the profiles of 11 possible aliases in 1-nm increments starting at 0, from +1 to +5, and then from −1 to −5 (only those Zeiss systems that coincide with a predicted alias are illustrated). These 11 aliases were constructed in a manner similar to that described in Experimental Characterization of LCSI Systems.

Alias Matching and Results

Figure 14 shows the aliases associated with the four systems that were extensively tested. One additional ZCSI system was evaluated only for aliasing, for a total of five systems. System Z1 was an almost perfect overlay with DRS Z + 0. Systems Z2 and Z3 shared a good fit with DRS Z-4, and system Z4 agreed well with DRS Z + 5. System Z5 (not shown in Fig. 14) was an almost perfect fit to DRS Z-2.

The alias for +2 nm, shown at the bottom of Table 11, predicts that a +2 nm wavelength offset from 0 could have the most dramatic affect on the spectral profile. Compared with system Z1 (matching to Z + 0) that has a WTWR of 0.74, a match to Z + 2 would produce a WTWR of 0.42 and the FWHM at 545 and 612 nm shifts from 20

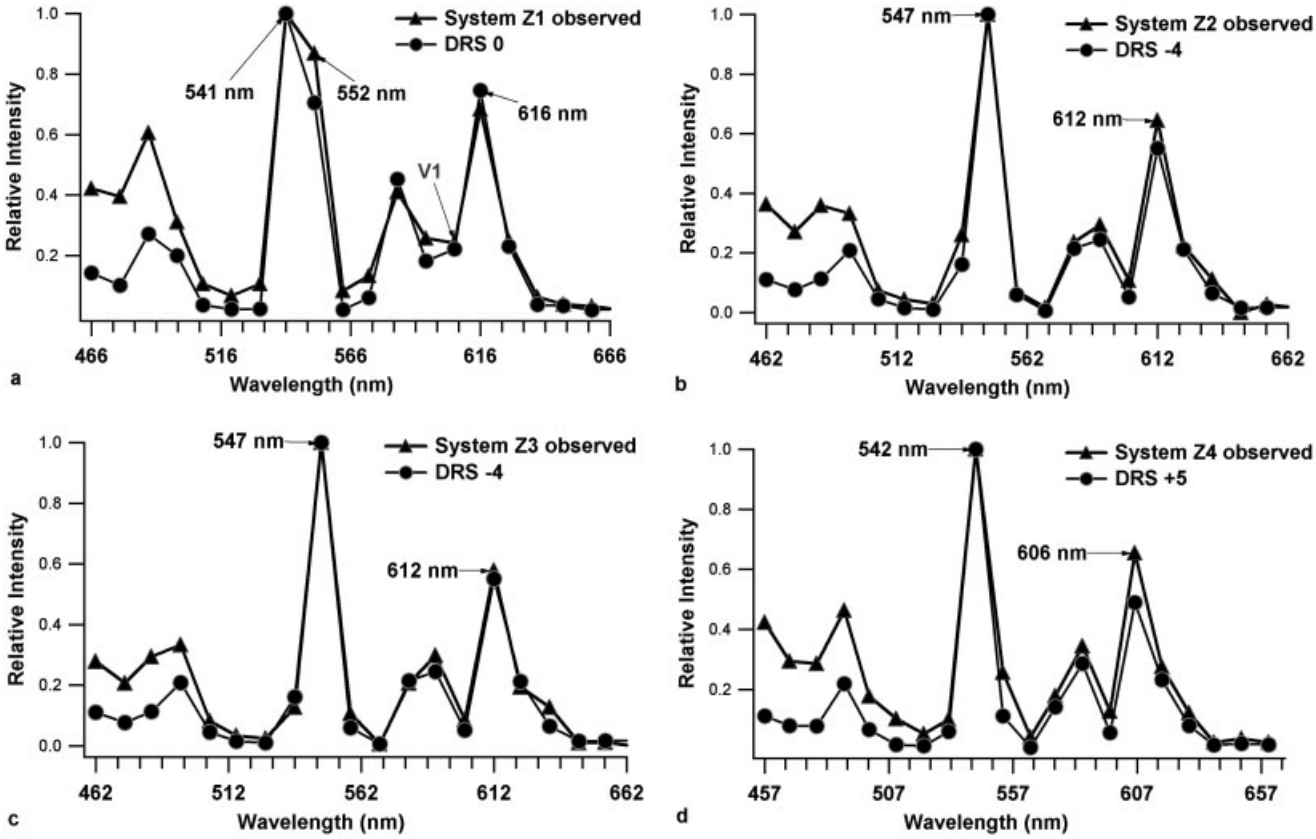

FIG. 14. Four aliases that best match the four ZCSI systems tested. Overall agreement between DRS predictions and actual spectral profiles is good, but each system presents differences in background in the blue. The width of the 545-nm feature and the depth of valley V1 show how the alias determines contrast and FWHM. The key lesson from this is that an emitted spectrum characterized on system Z1 may not present the same spectral profile as that produced by any other ZCSI system.

to 12 nm and from 15 to 28 nm, respectively. These are very significant spectral changes for only a 2-nm offset in the physical alignment! This shows that aliasing can be responsible for pronounced, nonintuitive, nonlinear changes in a spectral characterization. At the time of writing this report, we found no ZCSI system that presented the DRS L + 2 alias, but we have no reason to believe that it does not exist.

We found that the DRS and observed FWHM values agreed within experimental accuracy. WTWR agreement was good; however, PVR values were typically less than those predicted by the DRS profiles (except for system Z1), even though the morphology of the profiles fit quite well with the DRS (Table 11). We speculate that this was due to differences in the QE of the IPMT, scattered light, or cross-talk between and within individual IPMT detector elements. Wavelength accuracy was within expectations for a WSI of 11 nm for all the ZCSI instruments we tested.

Overall System Consistency

Because a small misalignment in the optical train or a rotation or translation error could produce the equivalent of a wavelength offset and a consequent change in spectral profile, we plotted a graph to determine the change in

Table 11
Comparison of Operating Parameters of Five Different ZCSI Systems

	WTWR		PVR		FWHM (F1-2)		FWHM (F1-4)	
System	DRS	Actual	DRS	Actual	DRS	Actual	DRS	Actual
Z1 (Z + 0)	0.8	0.8	4	3	19	20	15	15
Z2 (Z − 4)	0.6	0.7	13	6	12	13	14	15
Z3 (Z − 4)	0.6	0.6	13	7	12	11	14	12
Z4 (Z + 5)	0.5	0.7	10	6	12	13	15	15
Z5 (Z − 2)	0.7	0.9	10	7	18	15	14	14
Alias (Z + 2)	0.4		4		13		27	

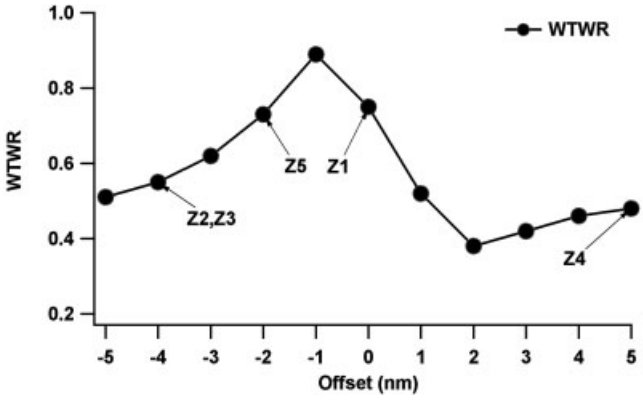

FIG. 15. WTRW values for the five ZCSI systems. Only systems Z2 and Z3 deliver the same wavelength ratios. The same experiment performed on systems Z1 and Z4 present different values. Standardization would enable all ZCSI systems to deliver essentially the same spectral profiles for a given experiment.

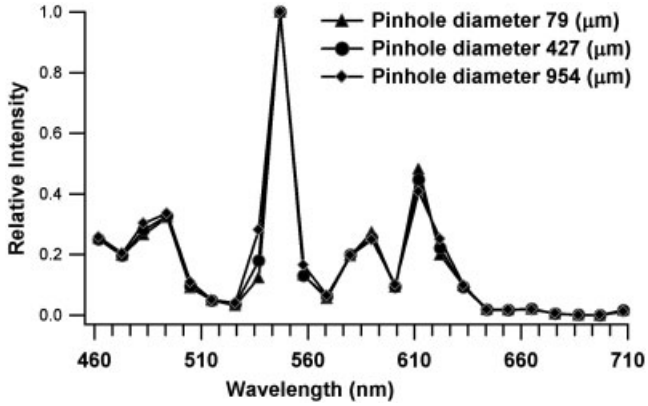

FIG. 17. ZCSI: pinhole diameter versus bandpass. In this case, bandpass does not change with pinhole diameter because individual elements of the IPMT are significantly larger than that of the pinhole. If the pinhole were to be opened larger that the width of an IPMT element, then the bandpass would degrade

wavelength ratios between Fl-4 and Fl-2 as a function of known wavelength offset (Fig. 15). It is evident that these systems were not set up to consistently re-create a standard spectral profile from a reference spectral calibration source. The net result is that it would be a matter of chance for one researcher to obtain the same wavelength ratios as another for the same experiment.

Characterization in the Red

The performance of system Z1 in the red when using the 766-nm RBF is shown in Figure 16. To acquire the spectrum, the power to the IPMT had to be significantly increased. The wavelength accuracy is within specifications, but the profile is asymmetric. Therefore, we would expect overlap with other fluorophores that emit in the same spectral region. The uneven distribution of energy also would result in lowered peak signal intensity and degradation in S/N ratio.

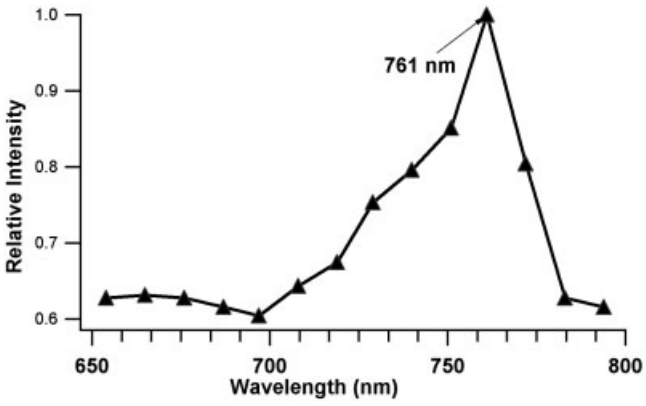

FIG. 16. A scan of the dielectric filter (RBF) with a 10-nm FWHM centered at 766 nm. System Z1 reported the FWHM to be 32 nm; however the asymmetry of the line profile implies the possibility of stray light or optical or electronic cross-talk in this region of the spectrum.

Effect of Pinhole Diameter on Performance

By using the MIDL as the calibration standard light source, the spectral range of 450 to 680 was characterized at 12 pinhole diameters (Fig. 17). From Spectrometer Design Fundamentals in the Appendix, we know that an image of the entrance pinhole is distributed across the detector elements of the IPMT at each wavelength present in the emission. A single monochromatic wavelength will result in a single image of the pinhole incident focused on a single detector element or could be split between two detector elements. Multiple monochromatic (or nearly monochromatic) spectral features such as those found in the MIDL will result in multiple images of the pinhole distributed across the IPMT.

Each of the 32 detector elements of the IPMT is 0.8 mm wide and on 1.0-mm centers located on the SDP (10). From the pinhole sizes listed in Table 12, the detector elements will always be considerably larger than the image of the pinhole. Equation 1 tells us that the bandpass (BP_{sw}) is determined by the wavelength dispersion multiplied by the effective aperture (W_{epa}), where the *effective* W_{epa} is larger than the exit aperture or the image of the entrance aperture (in this case, the entrance pinhole).

Because each detector element in the IPMT acts as an exit aperture and the image of the entrance pinhole is always smaller than the detector elements, we expect no change in spectral bandpass (BP_{net}) as a function of pinhole size up to ~1,000 μm. This was confirmed experimentally and is illustrated in Figure 17. Even though the difference between the smallest and largest pinhole exceeds a factor of 10, there is no evidence of a change in FWHM (spectral bandpass). The contributions of BP_{res} and BP_{nat}, which are components of the net bandpass (BP_{net}) in equation 2, are negligible compared with the magnitude of BP_{sw}.

However, this does not mean that increasing the size of the pinhole has no other effect on the profile of a spectral emission. We observed that increasing the pinhole diam-

Table 12
Pinhole Size Versus Pinhole Number for a Zeiss 10× Objective, 0.3 NA, in ZCSI System

Pinhole no.	1	2	3	4	5	6	7	8	9	10	11	12
Diameter (μm)	79	158	238	317	397	477	556	636	716	795	875	954

eter degrades the WTWR and PVR, as shown in Figures 18 and 19.

Discussion and Conclusions

We observed that the size of the detector pinhole has a negligible effect on bandpass with ZCSI systems. Therefore, even though the size of the pinhole will change as a function of the NA and magnification of the objective, the spectral resolution will remain constant because the detector elements of the IPMT are always significantly larger than the image of the pinhole (in this example, the W_{epa} is determined by the width of the detector elements). However, we observed that WTWR and PVR ratios degrade as the pinhole increases in diameter.

Only two of the five ZCSI systems shared the same alias, indicating that ZCSI systems are not aligned to a standard spectral source. Therefore, as we have seen with the MIDL tests, a spectral characterization made on one ZCSI system may not be duplicated on another. If an optomechanical error results in a wavelength offset of only 2 nm, wavelength ratios can change by as much as a factor of 2 when measured at peak intensity.

Because changing the pinhole size has no affect on FWHM but degrades WTWR and PVR values, it is advisable to work with the smallest pinhole that provides the best S/N ratio and spatial resolution.

OLYMPUS FV1000

After this report was near completion, we learned that Olympus had introduced a diffraction grating-based wavelength-dispersed CSI system with a 2-nm WSI called the FluoView1000 (OCSI). Olympus characterized the MIDL with one of its two spectral channels, and the result is shown in Figure 20. Each wavelength was acquired sequentially, comparable to that of an LCSI system.

When we compare this spectrum with that shown in Figure 1b, there is no evidence of aliasing. This is to be expected because of the 2-nm WSI and the large number of WDPs needed to cover the wavelength range from 400 to 650 nm. We also observe that the 405-nm Hg emission line is clearly visible, and the detail in the 611-nm feature confirms its excellent spectral resolution. The OCSI system presented the highest spectral resolution and the lowest background and aliasing of all the CSI systems we tested.

These results confirm that the MIDL is well suited as a diagnostic tool that can be used to characterize any confocal spectral system, especially those with the highest spectral resolution capabilities.

INTERFEROMETER-BASED SKY SYSTEM

The SKY interferometer system does not require a laser system for excitation and can operate in white light to perform brightfield spectroscopic measurements. Figure 21 shows a SKY interferometer scan of the MIDL.

The SKY system uses a Sagnac interferometer that acquires each wavelength sequentially over a fixed FOV. Each pixel in the camera acquires a complete spectrum per point on the FOV (16).

Results

The wavelength dispersion is nonlinear and requires more information than was available to enable us to construct DRS and show an overlay with theoretical DRS curves. However, the PVR was 6.6 and the WTWR was

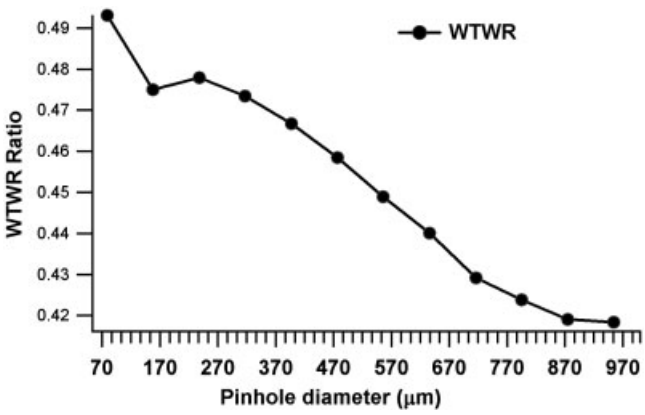

FIG. 18. Even though the bandpass does not change with wavelength, opening the pinhole with ZCSI systems changes WTWR values by ~15% from a pinhole diameter of 79 to ~900 μm.

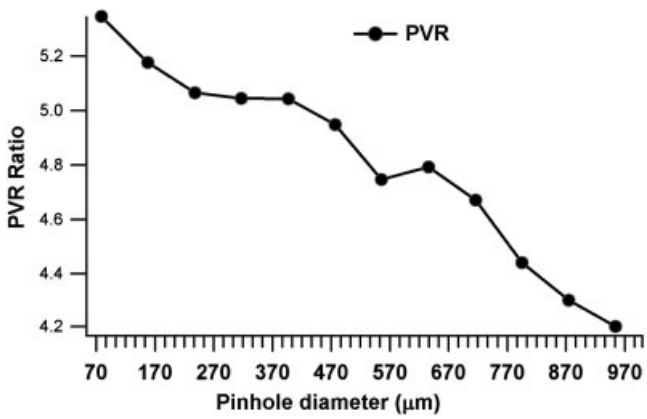

FIG. 19. As the pinhole diameter is increased in ZCSI systems, PVR values degrade by ~23% from a pinhole diameter of 79 to ~900 μm.

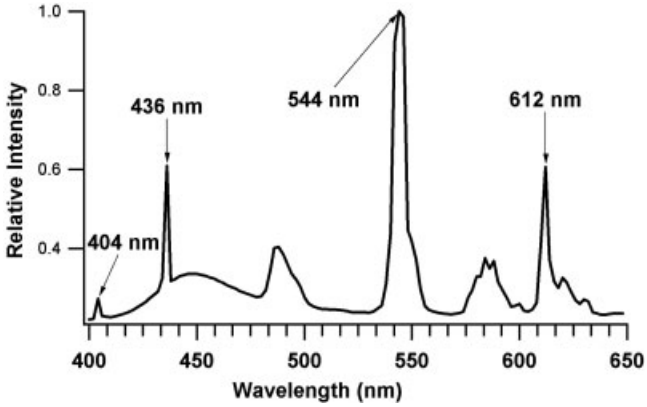

FIG. 20. MIDL scan acquired on an Olympus FV1000 with a WSI of 2 nm. The acquisition captured the 405-nm Hg line and spectral detail from 600 to 650 nm. As expected, there was minimal aliasing because of the low WSI value and the large number of WDPs required to cover the wavelength range.

0.45 versus 22 and 0.6 (Table 6) for a nonaliased LCSI system.

The WSI changes with wavelength in a nonlinear manner, so that a 436-nm WSI produces a 2.5-nm wavelength and a 612-nm produces a 4.2-nm wavelength. Even though the nominal FWHM and WSI are superior to those of the LCSI system, the contrast between Fl-3 (586 nm) and Fl-4 (611.5 nm) was less than expected when compared with a LCSI system (typically >10) as demonstrated by a PVR of only 6.6. Due to the symmetry of the spectral profiles, the low PVR value is more likely to be due to degraded spectral resolution or defocus rather than to scattered light. The wavelength accuracy was marginal to poor, given the low WSI values. Clearly, the MIDL provided a suitable means for characterizing and calibrating this instrument.

DISCUSSION AND CONCLUSIONS

We undertook this study to develop a simple and inexpensive means to characterize and validate the performance characteristics of any CSI system. In the absence of a stable reliable spectral calibration tool supplied by the manufacturer of our CSI system, we found that the spectral inconsistencies we observed in our own instrument were difficult to assess with accuracy or precision. The spectral characterization method we developed provides an absolute standard spectrum emitted by an MIDL that can be used to calibrate and confirm that a CSI system is performing consistently and correctly.

The MIDL makes it possible to differentiate between inherent systematic instrumental limitations such as undersampling errors (aliasing), optomechanical misalignment, and/or defocus. The suggested spectral characterization protocol provides a highly objective means of comparing the performance of like systems and of inconsistencies within the same system. We now know that the same or related model CSI systems can report the spectral profile of a MIDL differently. Depending on the PMT assembly used in an LCSI system, the spectral profile of the MIDL can change significantly even within the same system. This strongly suggests that multiple researchers running the same experiment could generate different data and may come to different conclusions simply as a result of instrumental inconsistencies and a lack of objective standardization.

By using an MIDL as a calibration and validation spectral source, we are guaranteed an absolute spectral standard that removes all issues associated with organic fluorophores and their inherent instabilities. The MIDL provides narrow spectral line widths that enable instrumental contributions to be easily observed and assessed. Because the integrity of a spectral image depends on the integrity of a spectral acquisition, broadened or inaccurate peak locations can be responsible for inferior performance.

As we expected, the systems with a WSI larger than 2 nm proved to be subject to aliasing, resulting in unexpected and nonlinear changes in the key properties of a spectral characterization, including wavelength ratios and contrast and spectral resolution. We also observed that the spectral profile of the MIDL presented by the OCSI system was virtually free of aliasing. We were also able to demonstrate that, regardless of the effects on spatial resolution, increasing the pinhole diameter changed WTWRs and degraded contrast. In addition, the spectral bandpass degraded in LCSI systems as a function of pinhole width (and we could expect the same for the OCSI system) but remained constant with the ZCSI system. In each case, we were able to show that observed spectral bandpass met theoretical expectations. Because the pinhole diameter is typically set to that of the Airy disk, and although it may be counterintuitive, spectral resolution actually degrades as spatial resolution increases, at least in LCSI and OCSI systems. There will be no adverse affect on spectral resolution in a ZCSI system, but we can expect that the LCSI, ZCSI, and probably the OCSI systems will to produce degraded WTWR and PVR ratios with an increase in pinhole size.

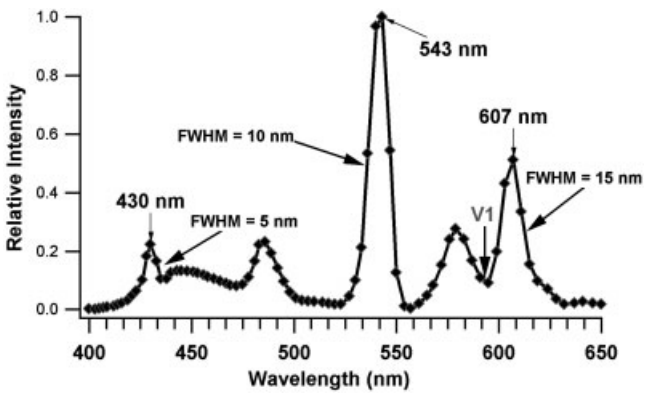

FIG. 21. Interferometer-based SKY system. As expected, the spectral scan of the MIDL presents nonlinear wavelength dispersion. The wavelength accuracy and PVR are less than expected because the average WSI value was ~4 nm.

Because the LCSI and ZCSI systems were prone to aliasing, we constructed simulated alias profiles for the MIDL and observed that real-life spectral scans from instruments in good alignment fit the predicted profiles very well. The use of predicted alias profiles enables unexpected variations in spectral profiles to be diagnosed as an expected inherent property of the instrument or as a malfunction.

Knowing the effects of aliasing on an MIDL spectral profile enables a researcher to optimize the instrumental setup by selecting the alias that results in the narrowest FWHM in the spectral region of interest. If all CSI systems of the same model were standardized to a single unique alias for a given WSI, then all similar systems could be expected to produce the same spectral profiles and wavelength ratios consistently across the confocal imaging community. If researchers published the MIDL spectrum as part of a calibration section of their findings, then other researchers could duplicate the same results by offsetting their system to operate with the same alias. With this technique, the FWHM of any spectral feature can be narrowed to the maximum extent possible. This may be less important for very broad fluorophores (>75 nm FWHM) but is critically important when working with fluorescent nanocrystal quantum dots and lanthanide quantum dyes because of their narrow spectral features or when multiple fluorophores overlap.

We hope that the confocal imaging community will adopt these or similar strategies to routinely calibrate, validate, and standardize the performance of their instruments. Standards enable communication, understanding, and the clear identification of shortcomings. As a final comment, we find it quite remarkable that no CSI manufacturer has provided a simple absolute means to enable a researcher to diagnose errors, measure accuracy, and confirm and validate the spectral capabilities of their instruments and the consistency of spectral characterizations. We hope we have provided a solution to this problem.

APPENDIX
Practical Considerations of the Optics of Spectroscopy and the Effect of Certain Hardware Features on the Performance of a CSI System

Spectrometer design fundamentals. The significance of how a spectrometer works and the influence of geometric optics on the performance of a CSI system cannot be overestimated. A CSI user who misunderstands the optics of spectroscopy may misinterpret spectral data and fail to optimize the performance of the CSI system. The following section is a tutorial that helps identify certain instrumental functions that inherently limit the ability of a CSI system to reconstruct a spectral profile. It also helps a CSI user to determine when an instrument fails to meet reasonable expectations.

The current spectrometric designs date to 1665, when Sir Isaac Newton described the optomechanical hardware of a spectrometer after he passed light through a prism and observed the splitting of light into colors. In 1821, Joseph von Fraunhofer was one of the first to custom design a ruling engine to produce diffraction gratings. By 1883, H. A. Rowland was "mass producing" these engines in plane and concave versions. Ready availability of diffraction gratings led to the Ebert spectrometer in 1889, a design that is still in use. Arnold Beckman, when faced with difficulty in obtaining diffraction gratings in 1942 during the Second World War, devised the prism-based Beckman DU that went on to become one of the most successful analytical instruments ever produced. Concave holographic gratings were introduced in 1971 and eliminated the need for any collimating or focusing optics (17,18); in 1992, the first confocal spectral imaging microscope system was developed based on a concave, aberration-corrected holographic diffraction grating (19). The dominant wavelength dispersive element (WDE) of almost all spectrometers remains a diffraction grating or a prism (20,21).

Two universal designs for prism and diffraction grating-based spectrometers are schematically illustrated in Figure A1. The configuration shown in Figure A1a is consistent with a ZCSI spectrometer and with the LCSI spectrometer shown in Figure 1Ab. These configurations image an entrance aperture, usually a slit in an analytical instrument, onto the SDP located at the focus of a mirror or lens following the WDE. An image of the entrance slit aperture appears at each wavelength in an emission spectrum. If the light emitted by the sample consists of a series of monochromatic spectral features, such as an MIDL, and the entrance aperture is a slit, then the spectrum will be observed as a series of "lines" on the SDP (hence, the term "spectral lines"). The physical width of each line will be no less than the width of the entrance slit aperture.

In a CSI system the entrance slit is replaced by a pinhole. A point on the FOV is imaged onto the pinhole aperture, which is then re-imaged through the spectrometer, is wavelength dispersed, and focused onto a detector. The size and shape of the pinhole are usually matched to the size of the image of the Airy disk to obtain the highest possible spatial and spectral resolution and the highest S/N. The image of the pinhole at the SDP will be observed as a series of circles, one for each monochromatic spectral feature, rather than as lines. The spectral resolution or bandpass of the system determines the ability of the system to resolve the physical overlap between two adjacent images of the pinhole at two different wavelengths. For example, if the spectral bandpass of the system is 5 nm, then it should be possible to resolve two spectral features separated by 5 nm by using the Rayleigh criterion (22). The ability of the spectrometer to determine the bandpass of an emitted spectral feature is *limited* by the WSI but is *not* determined by the WSI.

If the spectrometer is in "good focus," the image of the pinhole will be about the same height and width as the physical pinhole. The width (in millimeters) of the image of the pinhole contributes to the FWHM (also in millimeters) of a monochromatic spectral feature. White light incident on the pinhole will produce a continuous band of light, a "rainbow" limited by the spectral range emitted by

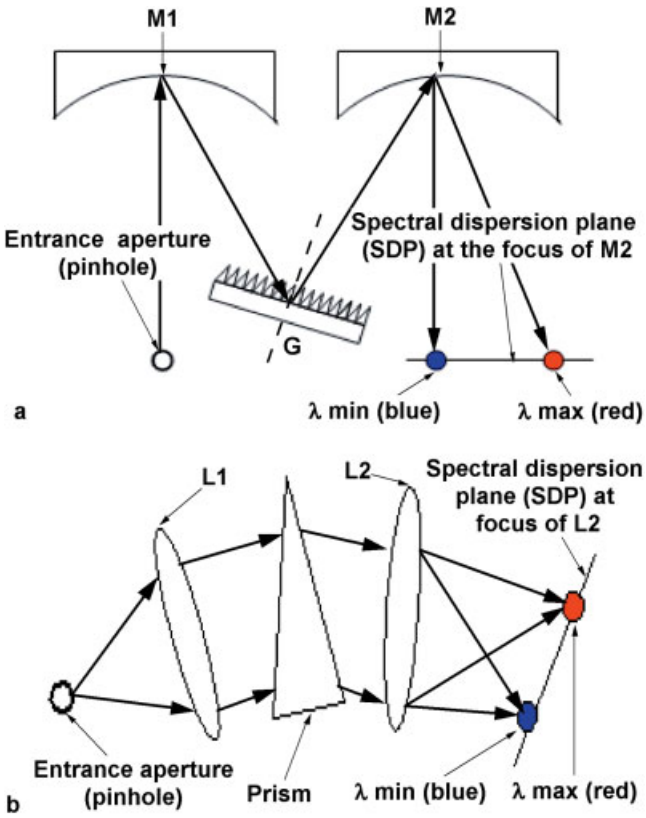

FIG. A1. Two common examples of the optical geometry of wavelength dispersive spectrometers: (**a**) a Czerny-Turner mount that uses a diffraction grating and is conceptually analogous to the ZCSI system and (**b**) a prism mount that is conceptually analogous to the LCSI system. In both cases, a pinhole entrance aperture is imaged (focused) with concave mirrors (M1, M2) or lenses (L1, L2) onto the SDP at each wavelength in a spectral emission. A ZCSI system focuses all wavelengths in the spectral range simultaneously across the 32 detector elements of an IPMT (~11 nm/element). An LCSI system acquires each wavelength sequentially by translating a slit assembly across the SDP (~5 nm/acquisition). Light passing through the slit is captured by a single PMT. PARISS places a CCD camera on the SDP to collect all wavelengths simultaneously.

the light source, with a height approximately that of the pinhole. A fluorophore would present a band of light whose length is dependent on the wavelength range present in the emission and the wavelength dispersion (in nanometers per millimeter) of the spectrometer at the SDP.

Although spectrometric designs have remained virtually unchanged for at least 100 years, the evolution of "flat" detectors such as linear silicon diode arrays, IPMTs (10), and CCD cameras required the spectrometer to present a flat, extended focal plane. The wavelength detector such as the IPMT in a ZCSI Zeiss system, a CCD camera for a PARISS system, or a translating slit assembly in an LCSI system are located at the SDP (22–24). The OCSI system is based on diffraction grating, and it acquires wavelengths sequentially; therefore, the diffraction grating rotates to change wavelength or the exit slit assembly translates. Each wavelength on the SDP is identified as a function of its physical location on the SDP. To determine the relation between distance (in millimeters) on the SDP and wavelength, the SDP must be calibrated by using a standard emission lamp such as the MIDL as the light source. A specific wavelength will then correlate with a specific column of CCD pixels, element of an IPMT, or a particular distance a slit must translate.

A fundamental difference between the CSI and all WDE spectrometers is their ability to acquire an emitted spectral range simultaneously in spectrographic mode (ZCSI and PARISS) or sequentially in "monochromator" mode (LCSI, OCSI, and the SKY interferometer system).

Optical subassemblies of CSI systems. Simplistically, all CSI system consists of four separate subassemblies: a microscope; a laser system that excites a "point" in the FOV that is imaged onto a matched pinhole (imaging a point onto a point); a classic confocal detection optical system that captures light from the point on the FOV and passes it through the pinhole, through a dielectric (barrier) filter, and then to a PMT; and a spectrometric system that collects light that passes through the pinhole and presents wavelength-dispersed light to a PMT or an IPMT. The PMT can be in the direct path of the dispersed light as in a ZCSI system or behind an exit slit aperture as in an LCSI system.

Spectrometric operating characteristics. The spectral resolution and spectral bandpass of wavelength-dispersive spectrometers depend on the following instrumental functions.

Wavelength dispersion. Wavelength dispersion controls the physical distance that separates one wavelength from another on the SDP and is a key parameter in determining the limits of spectral resolution. Wavelength dispersion is measured in nanometers per millimeter; hence, the smaller the number, the greater the physical distance that will separate two wavelengths at the SDP.

When designing an instrument, the overall wavelength dispersion is set by the width of the wavelength detector located on the SDP. For example, if a 32-mm IPMT is to acquire the entire spectral range from 400 to 750 nm simultaneously, then the wavelength dispersion must be 10.9 nm/mm ([750 − 400]/32), which is consistent with the specifications of a ZCSI system. Therefore, a 1-mm detector element on the IPMT will deliver a WSI of ~11 nm, with each detector element presenting 32 exit apertures. The WSI is analogous to the wavelength range that a barrier filter allows to pass and limits spectral bandpass but does not determine bandpass.

Spectral resolution and bandpass. Spectral resolution is defined as the absolute limit of an instrument's ability to separate two adjacent monochromatic spectral features emitted by a point in the FOV. The magnitude of spectral resolution is determined by the wavelength dispersion of the spectrometer and the sizes of the entrance and exit apertures. "Spectral resolution" becomes "spectral bandpass" when a spectrometer is deliberately operated at less than its resolution limit (a larger value in nanometers). In most analytical spectrometers, the bandpass is selected by changing the entrance slit width, and its spectral resolution is defined at its minimum slit width.

The limiting spectral *resolution* of an instrument is typically measured at the factory by acquiring the spectrum of a monochromatic light source with an entrance slit width of 10 μm or smaller (or a pinhole instead of a slit in a CSI system). The limiting resolution is then calculated by measuring the FWHM of the monochromatic spectral feature. The maximum *effective*, or observed, "resolution" of any spectrometer is determined by the FWHM by using the actual minimum slit width supplied with the instrument (which is almost never the narrowest slit that could be used with the instrument). The bandpass that the instrument operator selects will be determined by a slit width that is almost always wider than the slit width used for the limiting resolution measurement. High spectral resolution requires more WDPs than a low resolution system (greater wavelength sampling) and therefore is better able to detect subtle changes in the emission characteristics of a fluorophore. This is analogous to the flow cytometric FWHM that is used for calibration and system performance characterization (11,25,26). High spectral resolution better enables an instrument to handle commingled spectra (even if they are broad) and narrow emitters such as fluorescent nanocrystal quantum dots and lanthanide quantum dyes (27,28).

The operator of a CSI system typically has some control over the pinhole size, but changing the size of the exit aperture (either slit or detector element) may not be an option. It is important to be aware that changing the size of the pinhole or any spatial aperture (e.g., width of an exit slit assembly in an LCSI system to change the WSI) will change the bandpass and, hence, the observed line width of a spectral feature.

Calculating the FWHM. Once a spectrum has been digitized, software can calculate the FWHM. It can also be calculated manually by printing a hard copy of the spectral feature and then using a ruler to measure the distance between two wavelength increments on the abscissa about 50 nm apart. Determine the number of nanometers per millimeter. This is the relative linear dispersion. To determine the FWHM, measure the full width at half the height of a target spectral feature and multiply it by the relative linear dispersion. Because the wavelength dispersion of a prism system is nonlinear with wavelength, the relative linear dispersion should be calculated for two known wavelengths that are as close as possible to the spectral region of interest.

Calculating net spectral resolution and bandpass. The goal of any spectral imaging system should be to accurately reconstruct the true spectral profile of an emitting light source, not just its FWHM. Because the spectral profiles of chromophores and fluorophores can and do change as a function of pH, binding, ionization, and protein–protein interactions, it is important to be able to subtract or accommodate instrumental contributions and systematic errors to reveal the true spectral character of objects or areas in the FOV. Detailed spectral information enables a researcher to gain an insight into physiologic, physical, and chemical changes at the molecular level, and the inability to detect or recognize these changes can limit the usefulness of a CSI system.

By definition, a monochromatic light source has an infinitely narrow wavelength spread; therefore, from a naive perspective, an instrument characterizing such a source should present it with infinitely narrow width on the SDP. In reality, each "monochromatic" emission line is observed with finite physical width and FWHM at the SDP. These are determined by the width of the image at the entrance aperture and the wavelength dispersion of the spectrometer at the SDP. Therefore, characterizing a monochromatic light source is an excellent way to evaluate the real contributions to a spectrum due to instrumental parameters.

For a monochromatic light source, bandpass is simplistically determined by the wavelength dispersion of the WDE at the SDP and multiplied by the "effective" pinhole or slit aperture.

$$BP_{sw} = Disp \times W_{epa} \quad (1)$$

where

- BP_{sw} (nm/mm) is the bandpass determined by the width of the entrance aperture W_{epa} for the wavelength dispersion at a particular wavelength. In this case, it is calculated by measuring the FWHM of a monochromatic spectral feature emitted by a light source.
- Disp (nm/mm) is the physical distance that separates two wavelengths. In a diffraction grating-based system, this value is constant regardless of wavelength; however, Disp changes with wavelength in a prism-based system.
- W_{epa} (mm) is the *greater* of the width of the exit aperture or the image of the entrance aperture (in a CSI system, the entrance aperture will be the pinhole). The exit slit in an LCSI system will typically define the W_{epa}.

Equation 1 suggests that the ability of the spectrometer to measure the bandpass of an emitting source can be improved without limit by decreasing the W_{epa}. However, depending on the spectrometer and its wavelength range, the narrowest aperture will almost always be wider than 5 μm. The limiting resolution (BP_{res}) of a real-life system is determined by decreasing the exit slit or entrance pinhole widths (W_{epa}) until no further improvement in bandpass can be obtained.

The dispersion term (Disp) in equation 1 is approximately linear for a diffraction grating (dispersion varies with the cosine of the angle of diffraction) and is nonlinear for a prism (dispersion varies as the refractive index as a function of wavelength). For example, the wavelength dispersion for a prism may be 20 nm/mm at 440 nm and 60 nm/mm at 600 nm. This means that a 5-nm spectral segment centered at 440 nm would be spread over a physical distance on the SDP that is three times greater than that of a 5-nm segment centered at 600 nm. Therefore, to maintain constant bandpass in a prism-based LCSI

system, the effective exit slit width (not the entrance pinhole) should be three times wider at 440 nm than at 600 nm.

In a diffraction grating-based system, the difference in the cosine of the angles of diffraction from lambda maximum to minimum are small for a 12.5- or 17-mm CCD; therefore, wavelength dispersion can be considered to be constant. However, for a 32-mm IPMT, wavelength dispersion is nonlinear, which may be evident in the observed bandpass of the instrument as a function of wavelength (24).

If the light source is monochromatic and the goal is to increase the WSI from 5 to 10 nm, then the widths of the entrance pinhole and the exit slit should be doubled (in a ZCSI system, only the width of the pinhole can be changed). In practice, these parameters are not connected. Researchers select the sizes of the pinhole for spatial resolution and the WSI separately and independently, unless the WSI is otherwise fixed. The net result is that the WSI may underfill the exit slit in an LCSI system if the image of the pinhole is small or overfill the exit slit if the pinhole is large. In either case, there will be an effect on the S/N ratio, light throughput, and contrast.

Even if the source is a broad fluorescence emission rather than monochromatic light, the entrance pinhole and the exit aperture should be matched. Failure to do so results in compromised spatial and spectral resolution.

Purists should note that, to calculate the precise width of the image of the entrance aperture, it is necessary to multiply the ratio of the entrance arm length (the focal length of the collimating optic) and the exit arm length (the focal length of the focusing optic) by the ratio of the cosines of the angle of incidence and refraction at each wavelength. Because the SDP is a linear plane, it is a given that the exit arm length will change with wavelength for a fixed WDE (24).

Real-life bandpass determinations for polychromatic light. Equation 1 states that the BP_{sw} is determined by the dispersion characteristics of the WDE and the width of W_{epa}. However, in real life, when monochromatic light is absent, such as that emitted by a chromophore or fluorophore, the net bandpass (BP_{net}) is the FWHM of the convolution of the natural finite spectral bandwidth of the emitting source (BP_{nat}), the bandpass determined by the limiting aperture (BP_{sw}; from equation 1), and the limiting spectral resolution of the instrument (BP_{res}). It is wise never to assume that the limiting bandpass (resolution) of the instrument is small enough to be ignored.

Assuming a gaussian profile, the delivered net bandpass is calculated by:

$$BP_{net} = SQRT(BP_{nat}^2 + BP_{res}^2 + BP_{sw}^2) \quad (2)$$

where BP_{net} is the net delivered spectral bandpass, BP_{nat} is the natural bandpass of the emission line, BP_{res} is the limiting resolution of the spectrometer, and BP_{sw} is the bandpass determined by W_{epa}.

The *true* natural bandpass of a spectral emission can be calculated once the remaining parameters have been quantified. This relation works remarkably well even for the non-gaussian profiles typical of spectral features found in the life sciences. We use equations 1 and 2 to predict the bandpass characteristics of CSI systems in the main body of the report. Equations 1 and 2 enable an instrument operator to clearly compare those contributions that originate with the instrument with those contributed by the sample. If the natural FWHM of the emitting source is very small and the instrument is a high resolution system, then BP_{net} is determined almost entirely by the BP_{sw} and, hence, the effective width of the entrance aperture W_{epa}.

Effect of pinhole illumination on bandpass. We know from equations 1 and 2 that the width of the entrance aperture of the spectrometer (the pinhole in a CSI system) is a critical parameter for determining the ability of the instrument to measure the bandpass of an emitting source and thus the accuracy of a spectral characterization. In routine use, a CSI system matches the size of the pinhole to the size of the image of the excitation Airy disk (29–32), but sometimes compromises are made in which the pinhole is larger than the image of the Airy disk. This is especially the case for very weakly emitting fluorophores, when a researcher may open the pinhole to capture more light at the expense of spatial resolution.

Bandpass depends on the operating parameters of the objective. The influence of pinhole diameter on spatial resolution has been adequately described elsewhere (29). In most cases, the size of the pinhole is adjusted to the size of the Airy disk; therefore, in the simplest case, the size of the Airy disk has a direct effect on bandpass. In a laser-illuminated confocal system, the size of the Airy disk depends on the wavelength, magnification, and NA of the objective, as shown in equation 3 (3,4,29,32).

$$R_{opt} = A\lambda M/NA \quad (3)$$

where R_{opt} is the pinhole diameter, A is a constant, λ is wavelength, M is magnification, NA is numerical aperture, and $R_{opt} = W_{epa}$ (given the constraints described in Effect on Bandpass as a Function of Pinhole Diameter in a Confocal Configuration).

For example, the diameters of the pinhole reported by LCSI software (consistent with equation 3) are 79.5 μm for a 10×/0.4 NA lens and 151.5 μm for a 63×/1.32 NA lens at an excitation wavelength of 488 nm. Therefore, if we select a 63× lens rather than a 10× lens, the axial resolution will increase, but spectral resolution and bandpass will degrade by approximately a factor of 2 if we apply equation 1. When we apply equation 2 to a real-life experiment using the MIDL, we observe a 20% decrease in bandpass as predicted by equation 2 for an LCSI system (more on this in Characterization of ZCSI Systems). There will be no change in spectral resolution with the ZCSI system because W_{epa} is determined by the width of the elements of the IPMT and not the pinhole. In these examples, each lens fills the emission pinhole with light emanating from the excitation Airy disk at the sample. If the

research sets the pinhole to a size larger than the Airy disk, then bandpass will be determined by whether or not the pinhole is fully illuminated. Equation 3 also tells us that a 63×/1.32 NA lens will present greater spectral resolution than a 63×/1.2 NA lens because in this case R_{opt} (equivalent to W_{epa}) will be ~10% smaller than that for the lower NA lens.

Effect on bandpass as a function of pinhole diameter in a confocal configuration. A critical concern is the consequence of a pinhole that is always filled or partly filled by the image of an Airy disk on spectral bandpass. In theory, if a sample is rigorously nonscattering, then, from the point of view of the spectrometer, the effective size of the entrance aperture should be the size of the image of the Airy disk or of the pinhole, whichever is smaller. If the pinhole is opened so that the size of the pinhole is larger than the size of the image of the Airy disk, there should be no increase in light throughput because whatever photons are present are exclusively within the Airy disk. If the sample scatters light, then light throughput will continue to increase due to that scatter as the pinhole is opened.

Because the effective size of the pinhole is critical to bandpass and all samples scatter to a certain extent, we performed a light throughput test with samples of different scatter characteristics. If light increases continuously as the pinhole is opened, then we assume that the pinhole determines the size of the entrance aperture and not the size of the image of the Airy disk. In the case of a scattering sample, we expect some degree of nonlinearity because scatter decreases as the square of the distance from the Airy disk.

The following tests were performed on inverted Zeiss and Leica microscopes in standard confocal mode without wavelength scanning or zooming.

- Excitation source: Ar laser emitting at 488 nm
- Barrier filter and PMT assembly: The Leica system used the PMT 2 assembly and a wavelength region between 500 and 555 nm
- Microscope objective: A Leica plan apochromatic, 63×/1.32 NA, oil immersion lens with the back aperture fully open and filled with light or a Leica plan apochromatic, 10×/0.4 NA lens.
- Sample selection:

- Nonscattering: A front surface mirror.

Mildly scattering: A yellow magic marker smear was drawn across a coverglass (1.5 size, 0.17 mm) and glued to a 3- × 1-inch aluminum slide with a ½-inch hole in the middle. The yellow marking was on the side opposite that coated with immersion oil.

Very scattering: A yellow fluorescent plastic slide (Chroma Corporation) with immersion oil between the surface and a cover glass (1.5 size, 0.17 mm). The edges were sealed.

Extended source not limited by an Airy disk: The MIDL was positioned on the stage directly above the objective without oil.

Experimental protocol.

1. The objective lens was focused on the target surface to yield the maximum intensity with pinhole 1 to verify good focus.
2. The pinhole was then opened to its maximum value (600 μm for Leica, 1,000 μm for Zeiss) and the PMT voltage adjusted so that most pixels were slightly below saturation (mean ~220 GSU on a scale of 0 to 256). Care was taken to set the black scale value at a level that would ensure that all values across the pinhole ranges would be measured.
3. The pinhole size was then incrementally decreased in ~50-μm steps, and an image was stored for each pinhole size. Mean intensity values were obtained from a region of interest with a maximum number of pixels of relatively uniform intensity and converted into ASCII format by using the LCSI software or Image J for the ZCSI. The curves shown in Figure A2 were derived from the USEPA Leica system and were created in Excel after background subtraction and normalization to unity. Unless otherwise indicated, the 10× microscope objective described above was used.

Light throughput equation. To determine the degree to which a pinhole is illuminated, we must first determine the theoretical light throughput as a function of pinhole diameter. If light increases as theory predicts, then the pinhole is perfectly filled and the full diameter determines the theoretical bandpass. If light throughput fails to match theory, then the pinhole is partly illuminated and the bandpass will depend on the actually illuminated area and not on the physical diameter of the pinhole itself. Light throughput in any optical system depends on the area of the emitting source and the light collection cone (NA or F/number). Geometric light

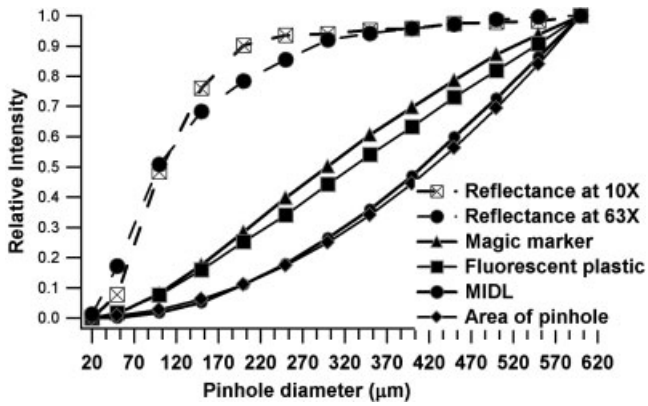

FIG. A2. Intensity versus pinhole diameter for various samples. The MIDL curve closely follows the curve for the area of the pinhole, as predicted by equation 4. The plots for the mirror form a plateau after reaching twice the size of the Airy disk with the 10× and 63× objectives. This indicates that the Airy disk determines the illuminated area. In the case of the scattering samples, the pinhole is nonuniformly filled, indicating that it is not possible to use the size of the Airy disk to determine the bandpass.

Table A1
Pinhole Diameter Versus Airy Disk (Pinhole Number) for Leica Plan Apochromatic, 10×/0.4 NA and 63×/1.32 NA

Airy disk (pinhole no.)	1	2	3	4	5	6	7
Diameter (μm)							
Airy disk 10×	79	151	239	318	398	476	557
Airy disk 63×	151	303	456	600			

throughput is variously called *étendue* or "geometric extent" and provides a means of determining relative light throughput for different optical systems by using equation 4. The value of L is a limiting constant for the *entire* optical system, whether for a spectrometer, a microscope, or a telescope.

$$L = \pi S\,(NA)^2 \qquad (4)$$

where S represents. Equation 4 assumes a conical beam and circular apertures. This equation explains why better telescopes rely on a large area for optimum light collection and microscopes rely on high NA.

Intensity versus pinhole for a nonscattering sample. When a sample is nonscattering, such as a front surface mirror, in laser confocal excitation, we expect that intensity will rapidly increase to a maximum as the pinhole is opened and then plateau when the size of the pinhole exceeds the size of the image of the Airy disk. This is exactly what we observed with a Leica 10×/0.4 NA dry lens and a Leica 63×/1.32 NA oil lens. The two upper plots with dashed lines shown in Figure A2 show that the smaller Airy disk associated with the 10× lens (open squares) reaches a plateau more rapidly than the larger Airy disk associated with the 63× lens (circles). However, both reach a maximum at about two times the nominal size of their respective Airy disks. In these cases, the bandpass of the system will be limited by the smaller size of the Airy disk or the pinhole. When the pinhole becomes larger than the Airy disk, the bandpass will reach a constant. Table A1 relates pinhole diameter to multiples of the nominal size of the Airy disk for 10×/0.4 NA and 63×/1.32 NA lenses.

Intensity versus pinhole diameter for scattering samples. The closer a curve follows the area of the pinhole (represented by diamonds in Fig. A2), the more scattering the sample and the more completely we would expect the pinhole to be filled. Figure A2 (using the 10× lens) shows that the curves for the magic marker (triangles) and the plastic slide (squares) are the same up to a pinhole size of ~150 μm (corresponding to two Airy disks); as the pinhole increases in size, the slopes of the two curves begin to diverge, with the thick plastic slide tending more toward the curve plotting the area of the pinhole than toward that of the magic marker. Clearly the thick plastic is more scattering than the magic marker, as we would expect. Neither the plastic slide nor the magic marker follows the intensity curve as a function of the area of the pinhole, indicating that the pinhole is nonuniformly filled and that the area of excitation is neither a "point" nor a homogenously extended illuminated area (such as a MIDL). Therefore, the bandpass of the system will degrade nonlinearly as the pinhole diameter is increased beyond the size of the Airy disk. The section Effect of Pinhole Diameter on Bandpass in Leica Systems in the main body of this report discusses actual examples of this effect. When scatter is a significant contributor to a net signal, linear unmixing algorithms may be compromised. For highly scattering samples, consider using nonlinear unmixing algorithms (15).

Intensity versus pinhole for an extended source. In this example, there is no Airy disk and the sample can be considered to be an "infinitely" scattering extended source. Therefore, the emitting area of the MIDL will fully illuminate the pinhole at all diameters, and its intensity curve should perfectly follow the area of the pinhole curve. This is shown in Figure A2 (solid line with circles). Therefore, given equations 1 and 2, we predict that the bandpass of the system will change directly with the pinhole diameter for any sample that is effectively an extended emission source. We show worked examples of pinhole diameter versus spectral resolution in Effect of Pinhole Diameter on Bandpass in Leica Systems.

Summary and conclusions.

1. Bandpass is defined as the ability of the CSI system to determine the FWHM of a spectral emission.
2. The bandpass of a CSI system is measured by using a light source that emits spectral features with very narrow FWHM (e.g., laser or MIDL). Equation 1 can be used to determine spectral resolution, and equation 2 can be used to determine the bandpass for an emitter such as a fluorophore presenting a wide FWHM.
3. The bandpass of a CSI system is a function of the effective width of the entrance aperture to the spectrometer (the diameter of the pinhole) or the width of a detector element, whichever is larger. Therefore, the bandpass of a ZCSI system is exclusively determined by the width of the detector elements because they are always larger than the pinhole.
4. With LCSI and OCSI systems, bandpass is determined by the pinhole diameter or by the width of the slit preceding the PMT.
5. For the LCSI and OCSI systems, the effective entrance aperture is determined by the pinhole or the Airy disk, whichever is smaller, for a nonscattering or nondiffusing sample such as a mirror reflector. For low scattering materials, the effective aperture is nonlinear with pinhole diameter; for highly scattering or diffusing samples, the effective width of the entrance aperture is the diameter of the pinhole regardless of the theoretical size of the Airy disk. Samples that scatter light nonuniformly fill the pinhole regardless of its diameter. In this case, bandpass will continue to degrade as the pinhole is opened. Bandpass will plateau with a reflective sample after the pinhole exceeds twice the size of the Airy disk.
6. The spectral resolution and bandpass (FWHM) in the LCSI and OCSI systems decrease as spatial resolution increases (higher magnification and NA). In the case of a

ZCSI system, spectral resolution and bandpass are unaffected by changes in spatial resolution because the size of an individual detector element is always larger than that of the pinhole.

7. Signal intensity is a function of the scattering properties of the sample. For a highly scattering sample such as a halogen lamp or MIDL, the signal strength increases in direct proportion to the area of the pinhole. The signal intensity of reflective samples plateau when the pinhole diameter exceeds twice the diameter of the Airy disk.

LITERATURE CITED

1. Trefethen LN. Maxims about numerical mathematics, computers and life. SIAM News 1998;31(1).
2. Zucker RM, Price OT. Practical confocal microscopy and the evaluation of system performance. Methods 1999;18:447–458.
3. Centonze V, Pawley J. Tutorial on practical confocal microscopy and use of the confocal test specimen. In: Pawley J, editor. Handbook of biological confocal microscopy. New York: Plenum Press; 1995. p 559–567.
4. Centonze V, Pawley J. Practical laser scanning confocal light microscopy: obtaining optimum performance from your instrument. In: Celis J, editor. Cell biology. New York: Academic Press; 1998. p 149–169.
5. Carter D. Practical consideration for collecting confocal images. In: Paddock S, editor. Confocal microscopy methods and protocols. Methods in molecular biology. Totowa, NJ: Humana Press; 1999. p 35–57.
6. Zucker RM, Price OT. Evaluation of confocal microscopy system performance. Cytometry 2001;44:273–294.
7. Dickinson ME, Bearman G, Tille S, Lansford R, Fraser SE. Multi-spectral imaging and linear unmixing add a whole new dimension to laser scanning fluorescence microscopy. Biotechniques 2001;31:1272–1278.
8. National Institute of Standards and Technology. Atomic spectra database: lines data; 2000.
9. Lerner JM, Drake L. Practical characteristics of spectral imaging methods. Am Biotechnol Lab 2002;20:36–40.
10. Multi-anode photomultiplier tube assemblies H7260 and H7260A. Tokyo: Hamamatsu Corporation; 2000.
11. Shapiro H. Practical flow cytometry. 3rd ed. New York: Wiley-Liss; 1995. p 106–135.
12. Tsien RY, Waggoner A. Fluorophores for confocal microscopy. In: Pawley J, editor. Handbook of biological confocal microscopy. New York: Plenum Press; 1995. p 127–137.
13. Proakis J, Manolakis D. Digital signal processing: principles, algorithms, and applications. New York: Prentice-Hall; 1996.
14. Castleman KR. Resolution and sampling requirements for digital image processing, analysis, and display. In: Shotton DM, editor. Electronic light microscopy. New York: Wiley-Liss; 1993. p 71–93.
15. Keshava N. A survey of spectral unmixing algorithms. Lincoln Lab J 2003;14:55–73.
16. Garini Y, Katzir N, Cabib D, Buckwald RA, Soenksen DG, Malik Z. Spectral bio-imaging. In: Wang XF, Herman B, editors. Fluorescence imaging spectroscopy and microscopy. New York: John Wiley & Sons; 1996. p 87–124.
17. Flamand J, Labeyrie A, Pieuchard G. Diffraction gratings. US patent no. 3,628,849; 1971.
18. Pieuchard G, Flamand J, Passereau G. Monochromator with concave grating. US patent no. 3,930,728; 1976.
19. Benedetti PA, Evangelista V, Guidarini D, Vestri S. Confocal-line microscopy. J Microsc 1992;165:119–129.
20. Loewen EG, Popov E. Instrumental systems. In: Diffraction gratings and applications. New York: Marcel Dekker; 1997. p 437–480.
21. Loewen EG, Popov E. Diffraction gratings and applications. New York: Marcel Dekker; 1997.
22. Hutley MC. Diffraction gratings. London: Academic Press; 1982.
23. James JF, Sternberg RS. The design of optical spectrometers. London: Chapman and Hall; 1969.
24. Lerner JM, Thevenon A. The optics of spectroscopy: a tutorial. Metuchen, NJ: Jobin Yvon/JY Optical Systems; 1998.
25. Robinson JP, managing editor. Current protocols in cytometry. In: Current protocols in cytometry. New York: John Wiley & Sons; 2000.
26. Zucker RM, Elstein KH, Gershey EL, Massaro EJ. Increased sensitivity of the Ortho analytical Cytoflurograph by modifying the fluidic system. Cytometry 1990;11:848–851.
27. Kim SM. Review on recent development of quantum dots: from optoelectronic devices to novel bio-sensing applications. In: Razeghi M, Brown GJ, editors. Quantum sensing: evolution and revolution from past to future. San Jose, CA: International Society for Optical Engineering; 2003. Vol. 4999 p 423–4330.
28. Lim YT, Kim S, Nakayama A, Stott NE, Bawendi MG, Frangioni JV. Selection of quantum dot wavelengths for biomedical assays and imaging. Mol Imaging 2003;2:50–64.
29. Wilson T. The role of the pinhole in confocal imaging systems. In: Pawley J, editor. Handbook of biological confocal microscopy. New York: Plenum Press; 1995. p 167–182.
30. Cogswell CJ, Larkin KG. The specimen illumination path and its effect on image quality. In: Pawley J, editor. Handbook of biological confocal microscopy. New York: Plenum Press; 1995. p 127–137.
31. Sheppard CJR, Shotton DM. Confocal laser scanning microscopy. Abingdon, UK: Bios Scientific Publishing; 1997.
32. Pawley J. Fundamental limits in confocal microscopy. In: Pawley J, editor. Handbook of biological confocal microscopy. New York: Plenum Press; 1995. p 19–36.